The Plant Cell, Vol. 26: 2486–2504, June 2014, www.plantcell.org

The bHLH142 Transcription Factor Coordinates with TDR1 to Modulate the Expression of *EAT1* and Regulate Pollen Development in Rice[C][W][OPEN]

Swee-Suak Ko,[a,b,1,2] Min-Jeng Li,[a,1] Maurice Sun-Ben Ku,[c] Yi-Cheng Ho,[c] Yi-Jyun Lin,[a] Ming-Hsing Chuang,[d] Hong-Xian Hsing,[a] Yi-Chen Lien,[a] Hui-Ting Yang,[a] Hung-Chia Chang,[a] and Ming-Tsair Chan[a,b]

[a] Academia Sinica Biotechnology Center in Southern Taiwan, Tainan 741, Taiwan
[b] Agricultural Biotechnology Research Center, Academia Sinica, Taipei 115, Taiwan
[c] Institute of Bioagricultural Science, National Chiayi University, Chiayi 600, Taiwan
[d] Department of Life Sciences, National Cheng Kung University, Tainan 701, Taiwan

Male sterility plays an important role in F1 hybrid seed production. We identified a male-sterile rice (*Oryza sativa*) mutant with impaired pollen development and a single T-DNA insertion in the transcription factor gene *bHLH142*. Knockout mutants of *bHLH142* exhibited retarded meiosis and defects in tapetal programmed cell death. RT-PCR and in situ hybridization analyses showed that *bHLH142* is specifically expressed in the anther, in the tapetum, and in meiocytes during early meiosis. Three basic helix-loop-helix transcription factors, UDT1 (bHLH164), TDR1 (bHLH5), and EAT1/DTD1 (bHLH141) are known to function in rice pollen development. bHLH142 acts downstream of UDT1 and GAMYB but upstream of TDR1 and EAT1 in pollen development. In vivo and in vitro assays demonstrated that bHLH142 and TDR1 proteins interact. Transient promoter assays demonstrated that regulation of the *EAT1* promoter requires bHLH142 and TDR1. Consistent with these results, 3D protein structure modeling predicted that bHLH142 and TDR1 form a heterodimer to bind to the *EAT1* promoter. EAT1 positively regulates the expression of *AP37* and *AP25*, which induce tapetal programmed cell death. Thus, in this study, we identified bHLH142 as having a pivotal role in tapetal programmed cell death and pollen development.

INTRODUCTION

Rice (*Oryza sativa*) is one of the most important staple crops in the world, feeding almost half of the world's population, and it serves as a model for monocots, which include many important agronomic crops (e.g., wheat [*Triticum aestivum*], maize [*Zea mays*], sorghum [*Sorghum bicolor*], and millet [*Setaria italica*]). The Food and Agriculture Organization of the United Nations predicts that rice yield will have to be increased 50 to 70% by 2050 to meet demands. Several approaches are currently adopted to increase rice yields, such as heterosis breeding, population improvement, wide hybridization, genetic engineering, and molecular breeding (Khush, 2000). Among these, hybrid rice is considered the most promising strategy, producing 15 to 20% increases in yield (Gao et al., 2013). Male sterility plays an important role in the development of hybrid crops, especially self-pollinated crop species. Male-sterile traits can be divided into cytoplasmic male sterility (CMS), which is determined by cytoplasmic factors such as mitochondria, and genetic male sterility (GMS), which is determined by nuclear genes. CMS has long been used in hybrid maize production, and both CMS and GMS are currently used for hybrid rice production (Luo et al., 2013). In the case of CMS-based hybrid crop production, a maintainer line is needed for the maintenance of the male sterile line.

Rice anthers are composed of four lobes attached to a central core by connective and vascular tissue. When anther morphogenesis is completed, microsporocytes form in the middle, surrounded by four anther wall layers: an epidermal outer layer, endothecium, middle layer, and tapetum (Goldberg et al., 1993). The tapetum is located in the innermost cell layer of the anther walls and plays an important role in supplying nutrients such as lipids, polysaccharides, proteins, and other nutrients for pollen development (Zhu et al., 2008). The tapetum undergoes programmed cell death (PCD) during the late stage of pollen development (Wu and Cheun, 2000); this PCD causes tapetal degeneration and is characterized by cellular condensation, mitochondria and cytoskeleton degeneration, nuclear condensation, and internucleosomal cleavage of chromosomal DNA. Tapetal PCD must occur at a specific stage of anther development for normal tapetum function and pollen development, and premature or delayed tapetal PCD and cellular degeneration can cause male sterility (Papini et al., 1999; Kawanabe et al., 2006; Li et al., 2006a; Luo et al., 2013).

Genetic and functional genomic studies of male sterility in *Arabidopsis thaliana* have shown that many transcription factors (TFs) play essential roles in pollen development and the regulation of tapetal PCD, such as mutations in *DYSFUNCTIONAL*

[1] These authors contributed equally to this work.
[2] Address correspondence to sweesuak@gate.sinica.edu.tw.
The author responsible for distribution of materials integral to the findings presented in this article in accordance with the policy described in the Instructions for Authors (www.plantcell.org) is: Swee-Suak Ko (sweesuak@gate.sinica.edu.tw).
[C] Some figures in this article are displayed in color online but in black and white in the print edition.
[W] Online version contains Web-only data.
[OPEN] Articles can be viewed online without a subscription.
www.plantcell.org/cgi/doi/10.1105/tpc.114.126292

TAPETUM1 (*DYT1*), *DEFECTIVE IN TAPETAL DEVELOPMENT AND FUNCTION1* (*TDF1*, *MYB35*), *ABORTED MICROSPORES* (*AMS*), and *MALE STERILITY1* (*MS1*); mutations in these factors all result in a male-sterile phenotype. The genetic regulatory pathway of pollen development suggests that *DYT1* (Zhang et al., 2006), *TDF1* (Ito and Shinozaki, 2002), and *AMS* (Sorensen et al., 2003) function at the early stage of tapetum development, while *AtMYB103/80* (Higginson et al., 2003; Phan et al., 2011) and *MS1* (Wilson et al., 2001; Ito and Shinozaki, 2002; Ito et al., 2007) play important roles in late tapetum development and pollen wall formation. In rice, several TFs, such as *UNDEVELOPED TAPETUM1* (*UDT1*; homolog of *DYT1*), are known to be key regulators of early tapetum development (Jung et al., 2005). In addition, mutations in *TAPETUM DEGERATION RETARDATION* (*TDR1*) (Li et al., 2006a), *GAMYB* (Aya et al., 2009; Liu et al., 2010), *ETERNAL TAPETUM1* (*EAT1*) (Niu et al., 2013), and *DELAYED TAPETUM DEGENERATION* (*DTD*) (Ji et al., 2013) all cause male sterility associated with tapetal PCD. *TDR1*, an ortholog of *Arabidopsis AMS*, plays an essential role in tapetal PCD in rice, and *tdr1* shows delayed tapetal degeneration and nuclear DNA fragmentation as well as abortion of microspores after release from the tetrad. Molecular evidence indicates that TDR1 directly binds the promoters of *CP1* and *C6* to regulate their transcription (Li et al., 2006a). CP1 is involved in intercellular protein degradation and its mutant shows defects in pollen development (Lee et al., 2004), and *C6* encodes a lipid transfer protein that plays a crucial role in the development of lipidic orbicules and pollen exine during anther development (Zhang et al., 2010a). EAT1 acts downstream of TDR1 and directly regulates the expression of *AP25* and *AP37*, which encode aspartic proteases involved in tapetal PCD (Niu et al., 2013). Microarray analysis of the coexpression gene networks during rice pollen development suggest that 108 genes may be involved in pollen wall synthesis and predicted that Os01g0293100 (*bHLH142* in this study) is directly connected to the expression of *CYP703A3*, *CYP704B2*, *MS2*, and *C6*, which may function in sporopollenin biosynthesis (Aya et al., 2011). Consistent with this, *cyp704B2* mutants showed swollen sporophytic tapetal layers, aborted pollen grains without exine, and undeveloped anther cuticles (Li et al., 2010).

The basic helix-loop-helix (bHLH) proteins are a superfamily of TFs and one of the largest TF families in plants. There are at least 177 *bHLH* genes in the rice genome (Li et al., 2006b; Carretero-Paulet et al., 2010) and more than 167 bHLH genes in the *Arabidopsis* genome (Bailey et al., 2003; Toledo-Ortiz et al., 2003). Generally, eukaryotic TFs consist of at least two discrete domains, a DNA binding domain and an activation or repression domain that operate together to modulate the rate of transcriptional initiation from the promoter of target genes (Ptashne, 1988). The bHLH TFs play many different roles in plant cell and tissue development as well as in plant metabolism. The HLH domain promotes protein–protein interaction, allowing the formation of homodimeric or heterodimeric complexes (Massari and Murre, 2000). They bind as dimers to specific DNA target sites and are important regulatory components in diverse biological processes (Toledo-Ortiz et al., 2003). So far, three bHLH TFs have been shown to be involved in rice pollen development: *UDT1* (*bHLH164*) (Jung et al., 2005), *TDR1* (*bHLH5*) (Li et al., 2006a), and *EAT1/DTD1* (*bHLH141*) (Ji et al., 2013; Niu et al., 2013).

By screening a T-DNA–tagged rice mutant pool of TNG67 (Hsing et al., 2007), we isolated a male sterility–related nuclear gene encoding a member of the bHLH TFs (*bHLH142*). In this study, we elucidate the molecular mechanisms underlying male sterility in this mutant. Our molecular and protein modeling results suggest that *bHLH142* is specifically expressed in the anther and bHLH142 coordinates with TDR1 in regulating *EAT1* promoter activity in transcription of protease genes required for PCD during pollen development. Therefore, we assert that bHLH142 plays an essential role in rice pollen development by regulating tapetal PCD.

RESULTS

Identification of a Male-Sterile Rice Mutant

From the T2 population of the Taiwan Rice Insertional Mutants (TRIM) lines, we identified a T-DNA–tagged rice mutant (denoted *ms142*) with a completely male-sterile phenotype. In the field, this mutant produced no viable seeds but maintained normal vegetative growth (Figure 1A) with panicles and spikelets developing similarly to those of the wild type (Figures 1B to 1D). The *ms142* mutant exhibits normal opening of spikelets and elongation of anther filaments (Figures 1D). However, the anthers of *ms142* were significantly smaller in size and appeared yellowish white (Figure 1D). The anthers of *ms142* could not be stained by Sudan black due to lack of lipid accumulation (Figure 1E) and showed no pollen grain development (Figure 1G).

Sequence Analysis of the T-DNA–Tagged Gene in the *ms142* Mutant

To determine T-DNA insertion copy number, DNA gel blot analysis of T2 mutant lines was conducted using *hptII* as a probe. Only a single band was detected in the mutant lines (Supplemental Figure 1A); thus, the mutation in *ms142* is due to a single T-DNA insertion. Analysis of the flanking sequence tag in the TRIM database suggests that *ms142* is a putative mutant with T-DNA inserted 1257 bp from the ATG start codon in the 3rd intron of *bHLH142* (RAP locus Os01g0293100, MSU locus Os01g18870). The protein encoded by this gene is annotated as a basic helix-loop-helix dimerization region bHLH domain–containing protein (RiceXPro, version 3.0). The *bHLH142* gene has four exons and three introns. Furthermore, genotyping by PCR using specific primers crossing the T-DNA insertion site verified its flanking sequence tag (Supplemental Figure 1).

Agronomic Traits of the *ms142* Mutant and Genetic Study

The agronomic traits of the mutant were examined in the selfed progenies of heterozygous mutants grown in the outdoor screen house. Heterozygous plants behaved similarly to the wild type in terms of vegetative and reproductive growth and produced fertile seeds. However, homozygous *ms142* mutant plants exhibited similar plant height, panicle number, and panicle length

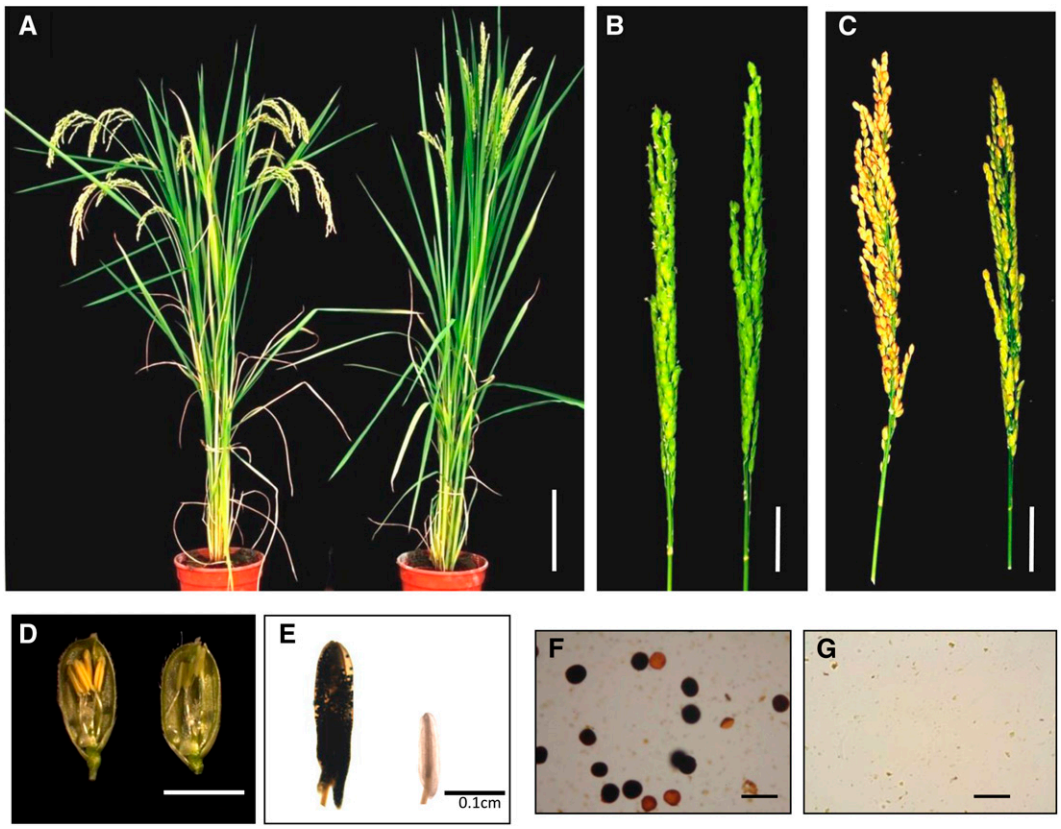

Figure 1. Phenotypic Analyses of *ms142* Mutant.

(A) Comparison of the wild-type plant (left) and *ms142* (right) after bolting.
(B) Comparison of the wild-type (left) and *ms142* (right) panicles at the heading stage.
(C) Comparison of the wild-type (left) and *ms142* (right) panicles at the seed maturation stage.
(D) Phenotype of the wild-type (left) and *ms142* (right) spikelets at one day before anthesis.
(E) Staining of anther by Sudan black in the wild-type (left) and *ms142* (right).
(F) Staining of wild-type pollen grains by I2/KI solution.
(G) Staining of *ms142* pollen grains by I2/KI solution.
Bars = 20 cm in **(A)**, 3 cm in **(B)** and **(C)**, 0.5 cm in **(D)**, 0.1 cm in **(E)**, and 20 μm in **(F)** and **(G)**.

to the wild type but produced no viable seeds (Supplemental Table 1).

To understand whether the sterility in *ms142* is due to male or female sterility, homozygous mutants were backcrossed with wild-type pollen. All F1 plants displayed wild-type-like growth and fertility. These results imply that the female organs of *ms142* develop normally. When the *ms142* BCF1 was selfed, the BCF2 progeny segregated into fertile and sterile plants in a ratio of 3:1 (Supplemental Table 2), suggesting that the male-sterile trait is controlled by a recessive gene. Consistent with the mutant phenotype, backcross segregants showed male sterility only in the homozygous plants, indicating that the male sterile phenotype cosegregated with the genotype. Moreover, when the selfed seeds derived from heterozygous plants of T2, T3, T4, and BCF2 generations were planted in different years and different cropping seasons, the scoring of the phenotype indicated that male sterility in *ms142* is stable and not affected by cropping season or year. Again, the fertile and sterile plants segregated in an ~3:1 ratio, as supported by χ^2 analysis (data for T4 and BCF2 shown in Supplemental Table 2). Taken together, these genetic analyses confirmed that the male sterility in *ms142* is controlled by a single recessive locus.

Defects in Anther Wall and Pollen Development in the *ms142* Mutant

To investigate the defects in the anthers of *ms142*, we examined the anatomy of anthers in the wild type and homozygous mutant. At the microspore mother cell (MMC) stage, the wild-type anther walls contained an epidermal cell layer, endothecial cell layer, middle layer, and tapetal cell layer (Figure 2A). During the early meiosis stage, the MMCs underwent meiosis to form tetrads of haploid microspores, the tapetal cells differentiated to form a large vacuole, and the middle layer cells began to degenerate (Figure 2B). At the tetrad stage, the meiocytes formed tetrads (Figure 2C). During the young microspore stage, free

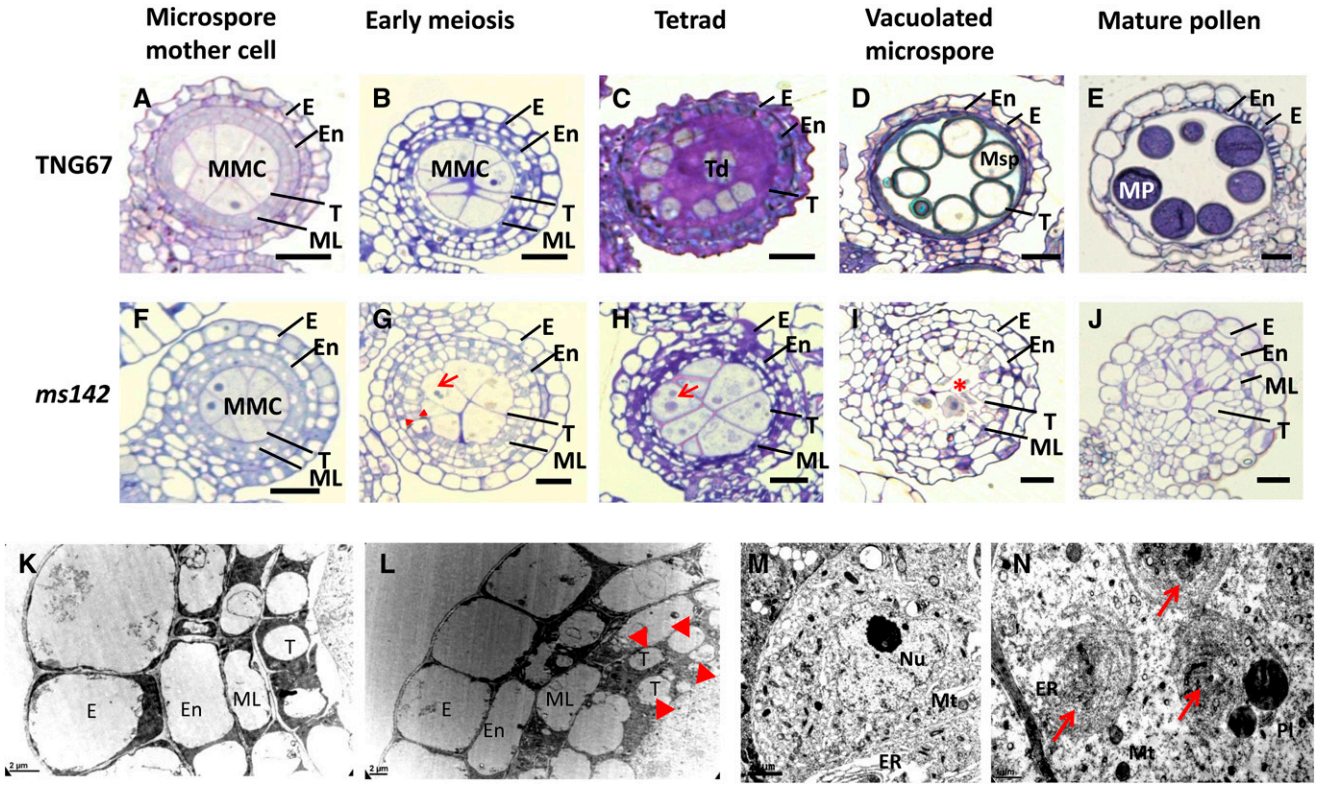

Figure 2. Transverse Anatomical Comparison of Anther Development in the Wild Type (TNG67) and *ms142* Mutant.

Semithin cross sections of wild-type (**[A]** to **[E]**) and *ms142* (**[F]** to **[J]**) anther at MMC, early meiosis, tetrad, vacuolated microspore, and mature pollen stages. TEM analysis of anther wall and microspore mother cell of the wild type (**[K]** and **[M]**) and *ms142* (**[L]** and **[N]**). E, epidermis; En, endothecium; ML, middle layer; T, tapetum; Td, tetrads; Msp, microspore; MP, mature pollen; Pl, plastid; Mt, mitochondria; Nu, nuclear; arrowhead, two tapetum layers; arrow, abnormal organelles; asterisk, degenerated microspore. Bars = 20 μm in **(A)** to **(J)**, 2 μm in **(K)** and **(L)**, and 1 μm in **(M)** and **(N)**.

microspores were released into the anther locule, and the microspores developed and exine was deposited on the pollen grain wall. The middle layers shrank and the tapetal cell layers became very dense (Figure 2D). At the mature pollen stage, the uninucleate pollen developed to trinucleate pollen with starch, protein, lipid, and other nutrients enriched in the pollen cytoplasm. At maturity, the tapetal cells were completely degenerated and the endothecial cell layers were thickening, ready for anther dehiscence (Figure 2E).

At the MMC stage, there were no visible differences in the anthers between the wild type and *ms142*. The *ms142* anther consisted of normal epidermis, endothecium, middle layer, and tapetum (Figure 2F). During the early meiosis stage, however, *ms142* MMCs did not enter meiosis and formed abnormal organelles (Figure 2G, indicated by arrow). Abnormal endoplasmic reticulum structure and apoptosis was also observed by transmission electron microscopy (Figure 2N, indicated by arrow). The *ms142* tapetal cells continuously became vacuolated and elongated, with some cells divided into two tapetal layers (Figure 2G, indicated by arrowheads). Transmission electron microscopy clearly showed two tapetal cells developed in the mutant (Figure 2L, indicated by arrowheads). The mid-layers of the mutant tapetum maintained their initial shapes, but meiocytes failed to divide into four cells at the tetrad stage (Figure 2H). The *ms142* mutant microspores finally degenerated during the vacuolated pollen stage (Figure 2I, indicated by asterisk). The tapetal and middle layer cells contained a large vacuole, and the middle layer cells did not degenerate (Figure 2I). Consequently, there were no mature pollen grains formed in the locules at the mature stage. The mutant anther wall still retained four to five layers of cells, i.e., epidermis, endothecium, middle layer, and one or two layers of tapetum cells. By contrast, the endothecial cell layer did not become thickened in the mutant even at the latter stage of anther development (Figure 2J).

Meiotic Activity in the *ms142* Mutant

Since early meiosis was arrested in *ms142* (Figure 2), we further performed meiotic analysis using acetocarmine to stain MMC chromosomes before meiosis (Chang et al., 2009b). The mutant exhibited no dyad development and meiocytes degenerated during meiosis; consequently, no microspore development was found in the mutant (Supplemental Figure 2A). By contrast, the MMCs of the wild type underwent normal meiosis and formed tetrad with four haploid cells and further developed into normal microspores.

To find out what caused retardation of meiocyte development in *ms142*, we compared the transcript levels of some meiosis regulatory genes by RT-PCR. The results indicated that *Mel1*, which functions in premeiotic germ cell division (Nonomura et al., 2007), was not significantly altered in *ms142*, while *PAIR1* (Nonomura et al., 2004), *PAIR3* (Yuan et al., 2009), and *SDS* (Chang et al., 2009a), important for chromosome pairing or synapsis during meiosis I, did not show any significant difference in expression between wild type and *ms142* (Supplemental Figure 2B). Therefore, the male-sterile phenotype in the mutant is not related to meiosis.

Mutated *bHLH142* Causes Defects in Tapetal PCD

Histological analysis indicated that *ms142* has abnormal anther morphology and aborted development of tapetal cells (Figure 2), which is not due to alteration in expression of meiosis-related genes (Supplemental Figure 2B). Thus, we suspected that mutation of *bHLH142* might cause altered tapetal PCD and thus affect tapetal degeneration (Papini et al., 1999). Tapetal PCD is characterized by cellular condensation, mitochondria and cytoskeleton degeneration, nuclear condensation, and internucleosomal cleavage of chromosomal DNA (Phan et al., 2011). Therefore, we performed a terminal deoxynucleotidyl transferase–mediated dUTP nick-end labeling (TUNEL) assay to detect DNA fragmentation in the anthers of the wild type and *ms142*. A TUNEL-positive signal began to appear in the tapetal cells of the wild type during meiosis and a strong TUNEL signal was detected during the young microspore stages (Figure 3). In contrast, no DNA fragmentation was observed in the tapetal layer in *ms142* throughout anther development (Figure 3). Differential interference contrast images of anther cross sections corresponding to TUNEL sections are shown in Supplemental Figure 3.

bHLH142 Is a Nuclear Protein

The gene structure of *bHLH142*, shown in Supplemental Figure 4A, indicates that the bHLH domain contains a bipartite nuclear localization signal (NLS), and the gene is predicted to encode a protein of 379 amino acids with a theoretical molecular mass of 40.7 kD and a pI of 6.2 (http://web.expasy.org/compute_pi). The predicted 3D protein structure of bHLH142 clearly shows the bHLH domain comprises two α-helices (Supplemental Figure 4C). Since the bHLH proteins are characterized as TFs, we assumed that bHLH142 is localized in the nucleus. To verify the subcellular localization, we constructed a fusion gene of the green fluorescent protein gene (*GFP*) and *bHLH142* under the control of the *35S* promoter and the *nos* terminator for transient expression in rice leaf mesophyll protoplasts (Supplemental Figure 4D). As a positive control, the *NLS* sequence was also fused to the red fluorescent protein (RFP) gene using the same regulatory elements. These constructs were introduced into rice protoplasts, and as expected, with the GFP construct alone, free GFP was found in the nucleoplasm as well as in the cytoplasm. However, the bHLH142:GFP fusion protein and the positive control of NLS:RFP were exclusively located in the nucleus (Supplemental Figure 4E). These results confirmed that, as a TF, bHLH142 protein localizes in the nucleus.

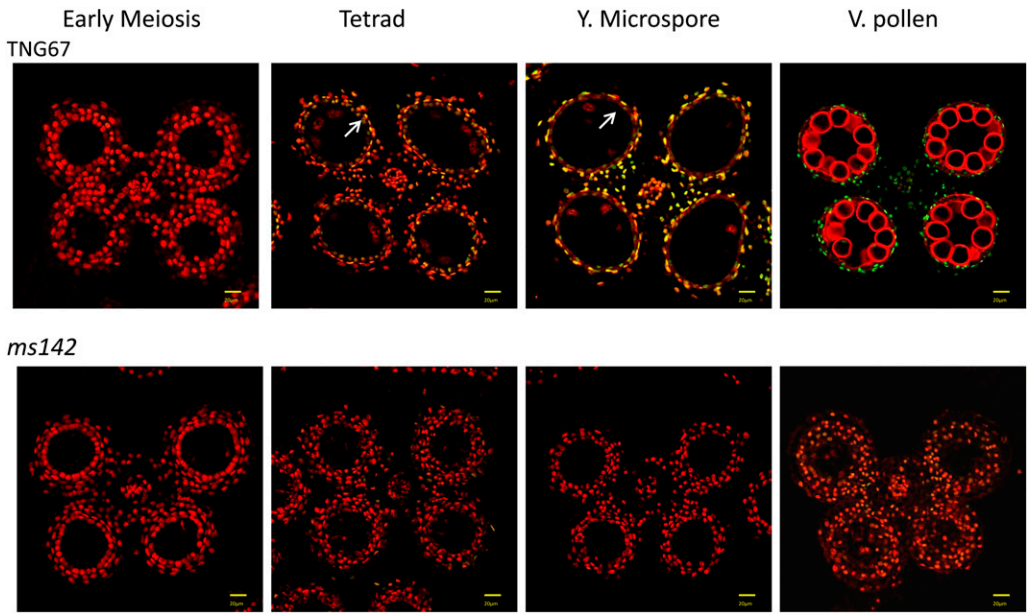

Figure 3. TUNEL Assay Showing Defected Tapetal Program Cell Death in the *ms142* Mutant.

DNA fragmentation signals (yellow fluorescence) started at the tetrad stage and exhibited obvious positive signals at the young microspore stage in TNG67. No DNA fragmentation signal was observed in the tapetum of *ms142*. The red signal is propidium iodide staining, and the yellow fluorescence is the merged signal from TUNEL (green) and propidium iodide (red). Bars = 50 μm.

Phylogenetic Analysis

To understand the evolution of *bHLH142* among various organisms, we used full-length bHLH142 protein sequence to search the National Center for Biotechnology Information BLAST database and retrieved 21 homologs containing the bHLH domain from 10 diverse terrestrial plants. The phylogenetic tree shows that UDT1 (bHLH164) and TDR1 (bHLH5) are in the same cluster, while rice bHLH142 and EAT1 (bHLH141) evolved and diversified into two separate clades. Phylogenetic analysis also suggests that bHLH142 is descended from a common monocot ancestor. Rice bHLH142 shares high sequence similarity with related proteins from *Brachypodium distachyon*, millet, *Triticum urartu*, maize, sorghum, and *Aegilops tauschii* (Supplemental Figure 5). The conserved homologs of bHLH142 from major cereal crops, such as maize, millet, sorghum, and wheat, share 84.1, 79.2, 72.2, and 78% amino acid sequence similarity to their rice counterpart (Supplemental Table 4). The maize homolog *GRMZM2G021276* (*ZmLOC100283549*) is highly expressed in immature tassel, meiotic tassel, and anther (http://bar.utoronto.ca/efp_maize/cgi-bin/efpWeb.cgi). In agreement, our RT-PCR data also verified that the maize homolog is tissue-specifically expressed in meiotic anther (data not shown). This result implies that the maize bHLH142 homolog may also play a similar role in anther and pollen development.

Expression Pattern of *bHLH142*

RT-PCR and quantitative RT-PCR (qRT-PCR) analyses of the wild type showed that *bHLH142* mRNA accumulates in young rice panicle and anther only, and not in other tissues (e.g., root, shoot, leaf, lemma, palea, ovary, and seed). In particular, high levels of transcripts were found in developing panicles (Figures 4A and 4B). Specifically, *bHLH142* transcripts were highly expressed in MMCs and extremely highly expressed in the anther at the meiosis stage, but this expression gradually decreased after the microspore stage (Figure 4C). Also, in situ hybridization (ISH) clearly demonstrated the specific expression of *bHLH142* in the anther but not in lemma and palea of wild-type spikelet at the early meiosis stage (Figure 4D). ISH with the cross sections of wild-type anther at various developmental stages showed positive signals in the tapetal layers at the early meiosis stage and in the tapetal layers and meiocytes during meiosis stage, with decreasing signals at the young microspore stage and negligible signals after the vacuolated pollen stage (Figure 5). Interestingly, the ISH signal was also detected in the vascular bundle (Figure 5), suggesting that the target genes of *bHLH142* might also be associated with nutrient acquisition in the anther. Conversely, there was no ISH signal detected in the anthers of the null mutant of *ms142* (Figure 5).

In addition, the expression patterns of various known pollen regulatory genes in the anther of the wild type versus *ms142*, as examined by qRT-PCR, confirmed the knockout of the *bHLH142* transcript in the *ms142* null mutant (Figure 6A). Also, expression of *TDR1*, *EAT1* (*bHLH141*), *AP37*, *AP25*, *CP1*, *CYP703A3*, *CYP704B2*, *MS2*, and *C6* was significantly downregulated in the *ms142* anther, relative to the wild-type anthers (Figures 6E to 6M). However, *MSP1* and *UDT1* transcripts were upregulated in the mutant at the MMC and meiosis stages (Figures 6B and 6C). There was no significant change in the *GAMYB* transcripts in *ms142* (Figure 6D). Interestingly, the extent of the suppression of *TDR1* expression (Figure 6E) in *ms142* was less than those of the other downstream genes (Figures 6F to 6M). To verify the gene hierarchy of *bHLH142*, we performed genetic study of *udt1* (TRIM), *eat1* (Tos17 mutant 'HA0530,' NIAS), and *ms142*. Our qRT-PCR results indicated that *bHLH142* is downregulated in the anther of *eat1* and *ms142*. Interestingly, knockout *UDT1* exhibited high accumulation of *bHLH142* in the early stage of MMCs. Taken together, these data suggest that *bHLH142* is located downstream of *UDT1* but upstream of *EAT1* (Supplemental Figure 6). In the *eat1* mutant, the expression of *CP1* was largely downregulated, while the expression of *C6* was not altered, suggesting that EAT1 may positively regulate the expression of *CP1* in addition to *AP37* and *AP25* (Supplemental Figure 6D).

bHLH142 and TDR1 Coordinately Regulate *EAT1* Promoter Activity

Based on the alterations in expression of known pollen regulatory genes in various mutants (Figure 6; Supplemental Figure 6), we assumed that bHLH142 might regulate *EAT1* promoter activity. Therefore, we performed transient promoter assays with the $EAT1_{pro}$-Luc construct. Our results demonstrated that bHLH142 or TDR1 protein alone cannot independently drive the expression of $EAT1_{pro}$-Luc. However, when combined, these two TF proteins together significantly increased Luc expression from the *EAT1* promoter by up to 30-fold. However, additional expression of EAT1 in the same cells reduced Luc expression from a 30-fold down to an 18-fold increase, presumably due to the competition between EAT1 and bHLH142 in binding to TDR1 (Figure 7). These results suggest that TDR1 and bHLH142 coregulate the activity of the *EAT1* promoter.

Protein Interactions between bHLH142, TDR1 (bHLH5), and EAT1 (bHLH141): Molecular Analysis

Next, we performed yeast two-hybrid (Y2H) analysis to determine whether bHLH142, as bait, interacts with the prey, TDR1 or EAT1. It was previously reported that full-length EAT1 and TDR1 proteins possess self-activation activity (Ji et al., 2013; Niu et al., 2013); our Y2H study also confirmed this phenomenon (Supplemental Figure 7A). Therefore, we also constructed a truncated $EAT1^{\Delta aa(1\text{-}254)}$ (truncated EAT1 at amino acids 1 to 254) and $TDR^{\Delta aa(1\text{-}344)}$ (truncated TDR amino acids at 1 to 344) to eliminate self-activation (Supplemental Figure 7A). Our results showed that bHLH142 is not self-activated (Supplemental Figure 7A); only the yeast strains coexpressing both bHLH142 and $TDR^{\Delta aa(1\text{-}344)}$ grew normally on stringent selection media (Figure 8A), and there was no direct interaction between bHLH142 and $EAT1^{\Delta aa(1\text{-}254)}$. Thus, bHLH142 did not directly interact with EAT1 (Figure 8A), and the retention of the C-terminal sequences of TDR1 is sufficient to confer the interaction of the two proteins. Clearly, the amino acid sequences in $TDR^{\Delta aa(1\text{-}344)}$ and $EAT1^{\Delta aa(1\text{-}254)}$ contain the interacting sites, consistent with the result of Ji et al. (2013). These results are further supported by the results of *EAT1* promoter assays in that both bHLH142

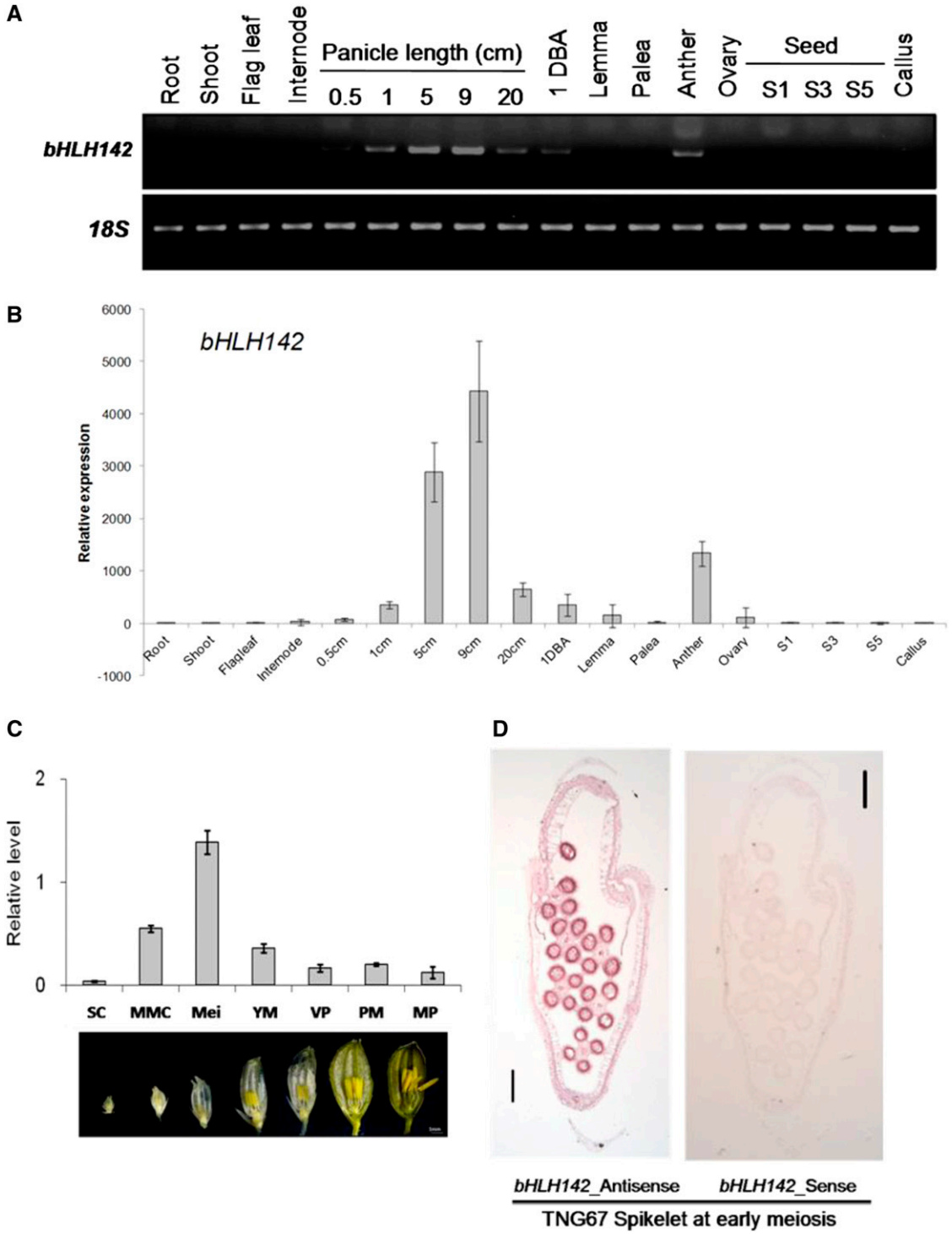

Figure 4. Tissue-Specific and Development-Dependent Expression of *bHLH142* in TNG67.

Spatial and temporal gene expression of *bHLH142* in various tissues of TNG67 (the wild type), as analyzed by RT-PCR **(A)** and qRT-PCR **(B)**. Expression of *bHLH142* in spikelet at various developmental stages in TNG67 **(C)**, and ISH of *bHLH142* antisense (left panel) and sense (right panel) probes in spikelet of TNG67 at meiosis stage **(D)**. Error bars indicate the SD of three biological replicates (**[B]** and **[C]**). DBA, days before anthesis; SC, sporogenous cell; Mei, meiosis; YM, young microspore; VP, vacuolated pollen; PM, pollen mitosis; MP, mature pollen. Bars = 1mm in **(C)** and 50 μm in **(D)**. [See online article for color version of this figure.]

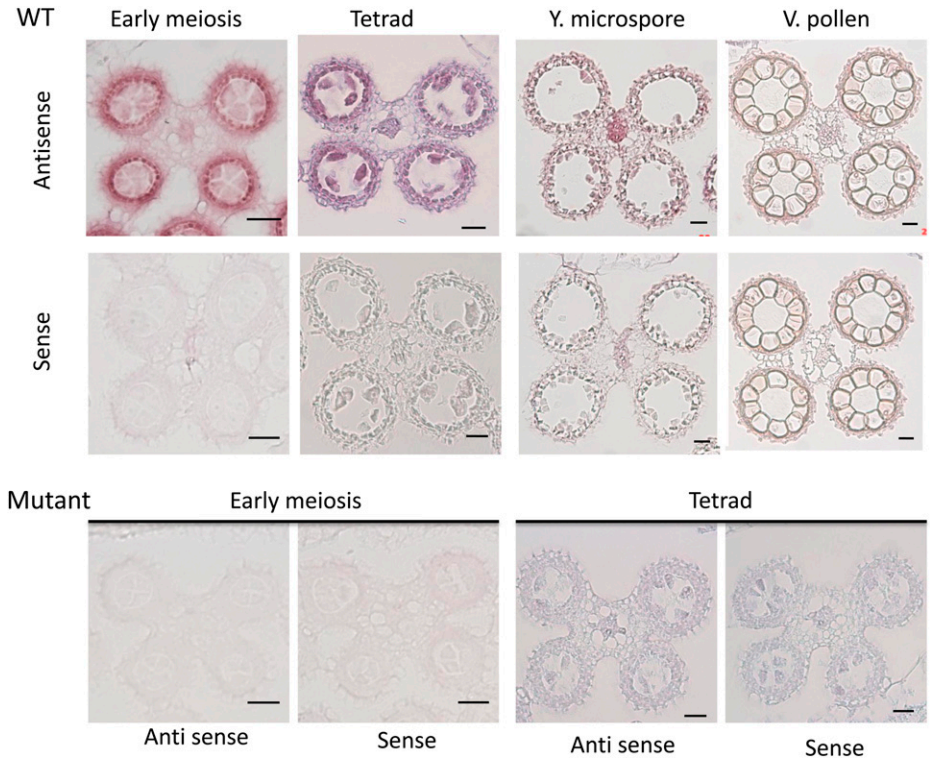

Figure 5. In Situ Hybridization Analysis of *bHLH142* Expression in the Anthers of the Wild Type and *ms142* Mutant at Various Developmental Stages.

Transverse sections of anther were hybridized with antisense or sense dig-labeled probe of *bHLH142*. Bars = 20 μm.

and TDR1 are required for the transcription of *EAT1* (Figure 7). Moreover, bimolecular fluorescence complementation (BiFC) assays showed that yellow fluorescent protein (YFP) signals are detected only in the nucleus of the rice cells coexpressing both NYN1-bHLH142 and CYN1-TDR1 (Figure 8B) and in the cells coexpressing both NYN1-TDR1 and CYN1-EAT1 (Figure 8B), but not in the cells coexpressing both NYN1-bHLH142 and CYN1-EAT1 (Supplemental Figure 7B). In vitro interaction of bHLH142 and TDR1 proteins was further validated by coimmunoprecipitation (co-IP), where interaction between hemagglutinin (HA) fused TDR1 and bHLH142 was confirmed (Figures 8C and 8D). Taken together, these molecular data provide solid evidence of the physical interaction between TDR1 and bHLH142.

Protein Interactions between bHLH142, TDR1 (bHLH5), and EAT1 (bHLH141): Protein Modeling

Molecular dynamic (MD) simulation was conducted to determine the protein–protein interaction between bHLH142 and TDR1 and to show how the heterodimer triggers the transcription of *EAT1* by binding to its promoter. The 3D structures of bHLH142, TDR1, and EAT1 were first obtained by ab initio protein modeling methods through MD simulation in an aqueous environment (Nelson et al., 1996). These proteins possess electrical and hydrophobic interactive surface patches for protein-protein interaction (Figures 9A and 9B). As shown in Figure 9C, bHLH142 interacts with TDR1 via these patches in the C-terminals to form an bHLH142/TDR1 heterodimer. The amino acid patches of ^{39}Asp-^{47}Trp, ^{236}Val-^{245}His, and ^{414}Met-^{462}Thr on TDR1 were predicted to bind to the corresponding patches of ^{19}Val-^{23}His, ^{38}Phe-^{66}Tyr, and ^{85}Gln-^{92}His on bHLH142 (Figure 9A) with a binding free energy of -3749 ± 30 kcal/mol. Furthermore, our modeling also demonstrated that EAT1, like bHLH142, binds to TDR1 at similar sites in the C-terminal regions (Figure 9C), with a binding free energy of -3325 ± 231 kcal/mol. Specifically, the amino acid patches of ^{41}Trp-^{47}Trp, ^{232}Ser-^{246}Ala, and ^{414}Met-^{460}Val on TDR1 were predicted to bind to the corresponding patches of ^{168}Leu-^{176}Ala, ^{198}His-^{220}Pro,^{274}Arg-^{282}Arg, and ^{309}Glu-^{319}Ile on EAT1 (Figure 9B). Again, EAT1 interacts with TDR1 to form an EAT/TDR1 heterodimer as bHLH142 does with TDR1, with a similar interface.

The bHLH protein surface grooves of bHLH142, TDR1, and EAT1 are rich in positively charged amino acids, and the grooves on the protein surface are possible regions for binding to the promoter of target genes. As both bHLHL142 and EAT1 are required to trigger the expression of *EAT1* (Figure 7), we analyzed the *EAT1* promoter sequence to identify the possible DNA binding sites. A total of 14 potential E-box binding sites (CANNTG) occur in the 2-kb promoter and 5′ untranslated regions (UTRs) of *EAT1*. One of these E-box *cis*-acting elements located on the promoter has a palindromic sequence (CAATTG) and is predicted to be the most favorable for binding to the dimer as it has a low free energy (Stormo and Fields, 1998). Our modeling predicted that the bHLH142/TDR1 heterodimer forms a DNA binding pocket along

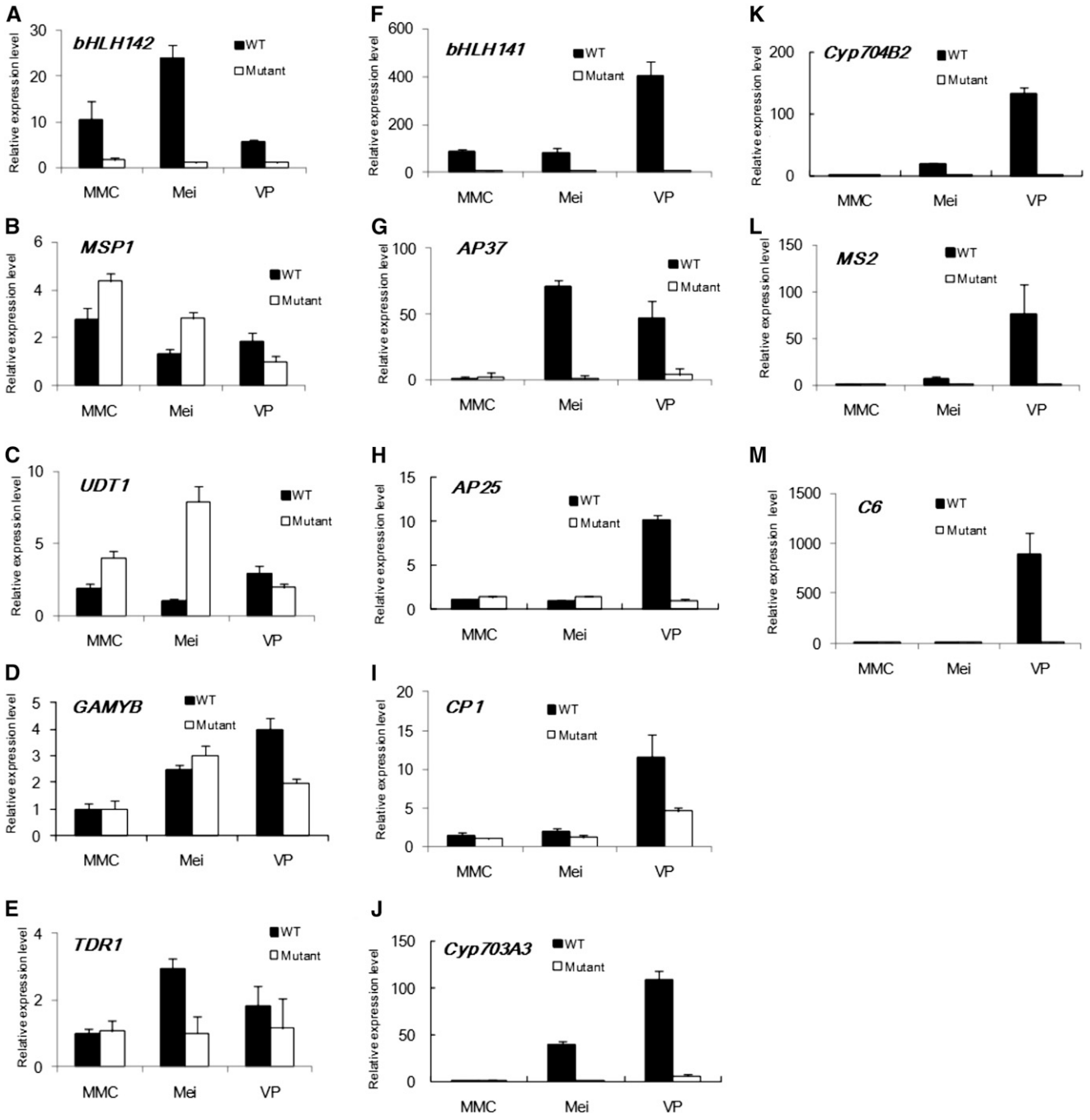

Figure 6. Analysis of Alteration in Expression of Key Regulatory Genes Involved in Pollen Development in *ms142* by qRT-PCR.

Error bars indicate the SD of three biological replicates. Mei, meiosis; VP, vacuolated pollen.

the edge of the dimer interface for binding to the E-box (CAATTG) of the *EAT1* promoter (Figure 10).

RNA Interference Transgenic Rice Lines Confirmed the Role of bHLH142 in Pollen Development

To further validate the biological function of *bHLH142*, we generated an RNA interference (RNAi) construct to suppress the expression of *bHLH142* in rice. The gene-specific region from the 5′ UTR of *bHLH142* was amplified, fused with β-glucuronidase (GUS) intron, and introduced into wild-type calli via *Agrobacterium tumefaciens*. All 16 T0 RNAi transgenic lines obtained had a male sterile phenotype similar to the T-DNA mutant *ms142*. These RNAi lines showed reduced expression of *bHLH142*, as examined by RT-PCR, and produced poorly developed anthers

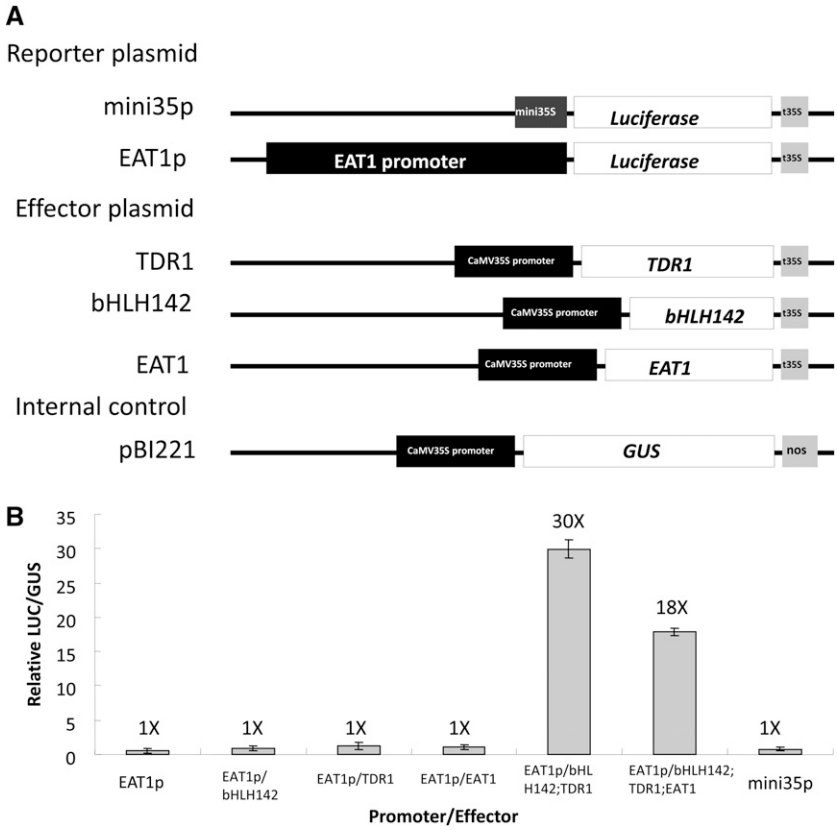

Figure 7. Coordinated Regulation of the *EAT1* Promoter by bHLH142 and TDR1.

(A) Schematic diagrams of the reporter, effector, and internal control plasmids used in the transient transactivation assay in rice leaf protoplasts. The reporter plasmid contains the CaMV35S minimal promoter and the *EAT1* promoter sequence (2 kb) fused to the firefly luciferase gene (*Luc*). In the effector plasmids, bHLH142, TDR1, and EAT1 genes are under the control of the CaMV35S promoter. Nos and t35s denote the terminators of nopaline synthase and CaMV35S, respectively. The *p*BI221 vector contains a CaMV35S promoter driving the expression of GUS as the internal control.
(B) Transactivation of the *Luc* reporter gene by bHLH142 and TDR in rice protoplasts. Different effectors were cotransfected with the reporter and internal control plasmid (*p*BI221). The data represent means of three independent transient transformations. Error bars indicate SD. Transient transformation without the effector plasmid (mini35p) was used as a negative control.

without pollen grains (Supplemental Figure 8). This result further supports the notion that bHLH142 plays a key role in rice anther and pollen development.

DISCUSSION

bHLH142 Is a Major Regulator of Rice Anther Development

Previously, three bHLH TFs were shown to be involved in pollen development in rice, and mutations of these TF genes all lead to complete male sterility. These genes are UDT1 (bHLH164) (Jung et al., 2005), TDR1 (bHLH5 (Li et al., 2006a), and EAT1/DTD1 (bHLH141) (Ji et al., 2013; Niu et al., 2013). They all play important roles in pollen development by regulating tapetal PCD. In this work, we identified a rice male-sterile mutant, *ms142*, with T-DNA inserted in the intron of *bHLH142*, which encodes another bHLH domain-containing TF protein. The *bHLH142* mutant phenotype is characterized by small anthers without pollen grain development (Figure 1). Genetic analyses suggested that the mutation is due to a single T-DNA insertion event. We further showed that this TF is located in the nucleus (Supplemental Figure 4) and plays an essential role in regulating rice pollen development. Close anatomical examination of anther development (Figure 2), TUNEL assay of DNA fragmentation (Figure 3), ISH gene localization (Figure 5), and expression of key gene transcripts (Figure 6) in the null mutant demonstrated that defects in microspore development are associated with defected tapetal PCD. Timely degradation of tapetum cells is essential for viable pollen development. Furthermore, suppressed expression of *bHLH142* in wild-type rice by RNAi confers the male-sterile phenotype (Supplemental Figure 8). Thus, this study shows the involvement of the bHLH TF bHLH142 in the dynamic regulation of pollen development in rice and likely in other plants as well.

Our analysis of expression profiles of known regulatory genes involved in pollen development demonstrated the downregulation of several genes, such as *TDR1*, *EAT1*, *AP37*, *AP25*, *CP1*, *CYP703A3*, *CYP704B2*, *MS2*, and *C6* etc., in *ms142* during pollen development (Figure 6). Therefore, we suggest that *bHLH142* participates upstream in the same regulatory pathway of anther development. A previous study reported that TDR1 positively

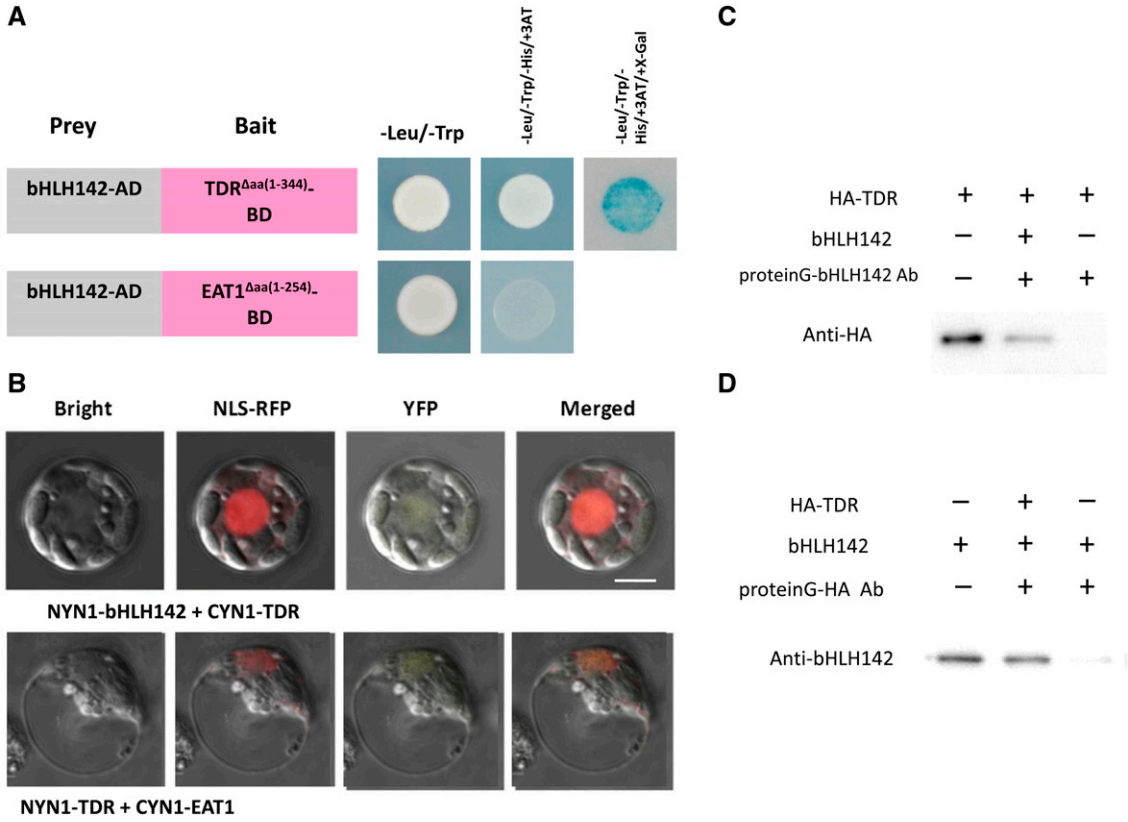

Figure 8. Interactions between bHLH142 and TDR1 and between TDR1 and EAT1.

(A) Y2H assays. Constructs expressing the full-length bHLH142 were cloned into the prey vector *p*GADT7 (AD) and truncated forms of TDR and EAT1 were introduced into the bait vector *p*GBKT7 (BD), respectively. Yeast strains were tested for growth in selective medium lacking Leu, Trp, and His and supplemented with 3-amino-1,2,4 triazole and X-Gal.

(B) BiFC in rice protoplasts expressing the indicated constructs. The top panel shows bHLH142 protein interacted with TDR in the nucleus. The bottom panel shows TDR interacted with EAT1 in the nucleus. NLS-RFP was used as nuclear localized control. Bar = 10 μm.

(C) Co-IP assay of HA fused TDR and bHLH142 recombinant proteins expressed in *Escherichia coli*, pulled down by protein G fused with bHLH142 antibody, and detected using anti-HA antibody.

(D) Co-IP assay of HA fused TDR and bHLH142 recombinant proteins expressed in *E. coli*, pulled down by protein G fused with HA antibody, and detected using anti-bHLH142 antibody.

regulates *CP1* and *C6* (Li et al., 2006a), and a more recent study suggested that EAT1 regulates the expression of two aspartic protease genes, *AP25* and *AP37* (Niu et al., 2013). However, our data suggest that EAT1 may also directly regulate the expression of *CP1* (Supplemental Figure 6D). Ji et al. (2013) reported that mutation in *DTD* (an analog of *EAT1*, *bHLH141*) in rice results in severe male sterility. The *eat1* or *dtd* mutant undergoes a normal meiosis process but *ms142* cannot proceed beyond meiotic cell division (Supplemental Figure 2). Similar to *udt1* (Jung et al., 2005), *ms142* meiocytes did not develop to microspores, while mutants of *TDR1* in rice and its homolog *AMS* in *Arabidopsis* showed thickened tapetum and microspore degeneration after release from tetrads (Sorensen et al., 2003; Li et al., 2006a).

Our transmission electron microscopy (TEM) examination demonstrated abnormal endoplasmic reticulum (ER) and apoptosis in MMCs of *ms142* mutant at the early meiosis stage (Figure 2N). This implies that *bHLH142* might play an extra role in meiocyte development. So far, very little has been reported on ER apoptosis in relation to plant pollen development. The ER functions in the synthesis and folding of proteins. Correctly folded proteins exit the ER and transport to the Golgi and other cellular compartments. Misfolded proteins may accumulate in the ER and cause stress to the cells. In response, cells may activate the unfolded protein response to maintain homeostasis of proteins in the ER. If the unfolded protein response is not sufficient to recover normal ER function, cells die by apoptosis (Rasheva and Domingos, 2009).

Our ISH analysis revealed that as well as being expressed in the tapetal layer, *bHLH142* is also expressed in meiocytes as well as in the vascular bundle (Figure 5). These results suggest that *bHLH142* might also play an additional role in nutrient acquisition during microspore development. Our qRT-PCR data demonstrated that expression of *CYP703A3*, *CYP704B2*, *MS2*, and *C6* is significantly downregulated in *ms142* anthers (Figure 6), confirming the prediction of a coexpression network by Aya et al. (2011). Therefore, our data support the notion that

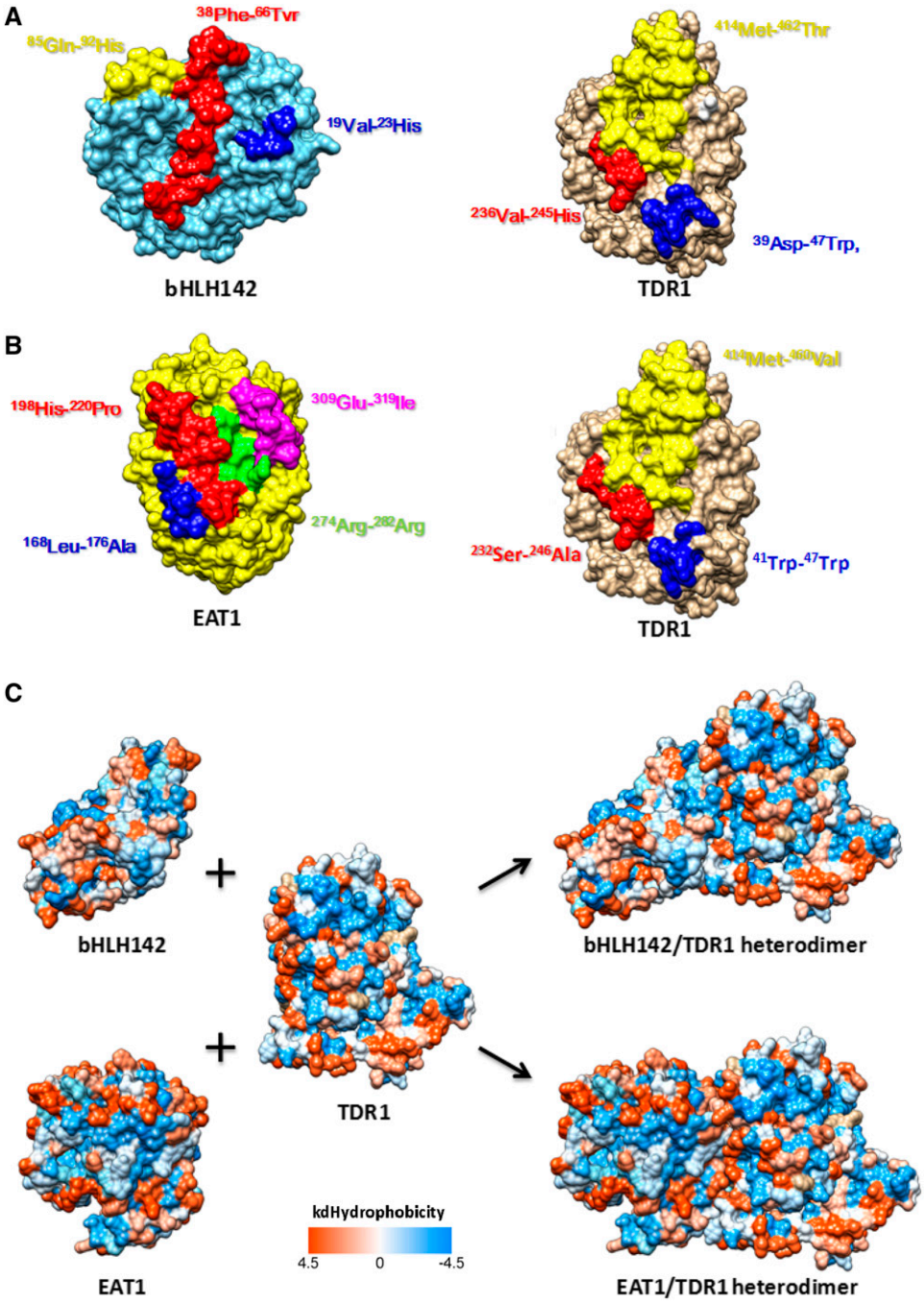

Figure 9. Molecular Dynamics Simulations of Protein–Protein Interaction between bHLH142 or EAT1 and TDR1.

(A) Predicted amino acid patches on bHLH142 and TDR1 that form protein–protein interactions.
(B) Predicted amino acid patches on EAT1 and TDR1 that form protein–protein interactions.
(C) The predicted heterodimers of bHLH142/TDR1 and EAT1/TDR1.
The 3D structure modeling indicated that both bHLH142 and EAT1 bind to TDR1 at the same region in the C termini and form a similar interface.

bHLH142 plays an additional role in the sporopollenin biosynthesis pathway.

This study uncovers bHLH142 as a bHLH TF family factor that is critical for pollen development alongside UDT1 (bLHL164), TDR1 (bLHL5), and EAT1 (bHLH141). Our data suggest that bHLH142 acts downstream of UDT1 (bHLH164) but upstream of TDR1 (bHLH5) and EAT1 (bHLH141) (Figure 6). Interestingly, all four bHLH TFs are expressed specifically in the anther and

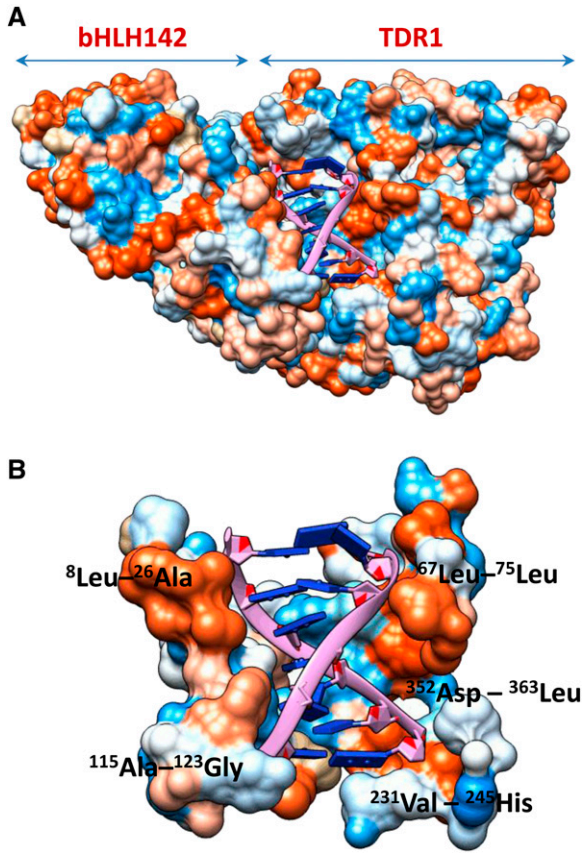

Figure 10. The Predicted bHLH142/ TDR1 Heterodimer and Its Binding to the Specific Region on the Promoter of *EAT1*.

(A) The TDR1/bHLH142 heterodimer binds to an E-box (CAATTG) on the *EAT1* promoter, with the E-box fitting to the pocket center at the interface of the heterodimer.

(B) The 6-bp E-box (CAATTG) binds to TDR1 at ^{67}Leu–^{75}Leu, ^{231}Val – ^{245}His, and ^{352}Asp – ^{363}Leu and to bHLH142 at ^{8}Leu–^{26}Ala and ^{115}Ala–^{123}Gly.

participate in sequential pollen development events, particularly in tapetal PCD. Several of the bHLH TFs act coordinately in regulating anther development, and it is thus likely that more TFs are involved in controlling the regulatory network to ensure normal pollen development.

Also, we noticed that there was lower level of expression of *TDR1* in *ms142* compared with the other downstream genes in the regulatory network. This may be attributed to the fact that TDR1 is also known to be regulated by another TF, GAMYB (Liu et al., 2010). In agreement with this finding, the expression of *GAMYB* was not altered in *ms142* (Figure 6). Taken together, these results suggest that two parallel pathways may exist in the regulatory circuit leading to TDR1 during pollen development.

bHLH142 Functions Coordinately with TDR1 to Regulate the *EAT1* Promoter

Transcripts of *TDR1* and *EAT1* are both downregulated in the *ms142* (Figures 6E and 6F). We hypothesize that TDR1 interacts with bHLH142 and positively regulates *EAT1* expression and thus the transcriptional activities of *AP25* and *AP37*, which encode aspartic proteases for tapetal PCD. Our promoter transient assay provides solid evidence that bHLH142 and TDR1 work coordinately in regulating the *EAT1* promoter (Figure 7). We also demonstrated that additional expression of the EAT1 protein significantly reduced *EAT1*-Luc promoter strength from a 30-fold increase down to an 18-fold increase (Figure 7), which may be attributed to the competition between bHLH142 and EAT to interact with TDR1. Presumably, more EAT1 favors the TDR1/EAT1 interaction and might consequently reduce the interaction between bHLH142 and TDR1, therefore reducing *EAT1* transcriptional activation (Figure 7). Our data suggest that bHLH142 interacts with TDR1 to coregulate *EAT1* expression.

Our molecular studies provide solid in vivo (Y2H and BiFC) and in vitro (co-IP) evidence that bHLH142 and TDR1 proteins interact (Figure 8). The co-IP provides convincing evidence that these two proteins physically interact in vitro. Subcellular localization also demonstrates that bHLH142 protein is localized in the nucleus (Supplemental Figure 4; Figure 8B) and its protein is not self-activated (Supplemental Figure 7A). Since we also found self activation of full-length TDR1 and EAT1 in our Y2H experiment (Supplemental Figure 7), N-terminal truncated forms of TDR$^{\Delta aa(1-344)}$ and EAT1$^{\Delta aa(1-254)}$ were used in our experiments to reduce self-activation. These two N-terminal truncated protein forms did not exhibit self-activation in yeast cells (Supplemental Figure 7A). Therefore, we are confident that bHLH142 interacts with TDR1 by using these truncated proteins to eliminate the bias (Figure 8). Our data indicate that bHLH142 interacts with TDR1 in the C-terminal (Figure 8) and support the conclusion of Ji et al. (2013) that DTD/EAT1 (bHLH141) interacts with TDR1 in the C-terminal region. In other words, both bHLH142 and EAT1 (bHLH141) can interact with TDR1 in the C terminus of TDR1. This finding also supports the result of our *EAT1* promoter assay, which showed that additional EAT1 protein reduced *EAT1* promoter activity, presumably due to the competition between bHLH142 and EAT1 proteins in the C terminus of TDR1.

From the 3D modeling, it is clear that bHLH142, EAT1, and TDR1 all have electrical and hydrophobic interactive surface patches in the C-terminal region for protein–protein interaction (Figure 9). Both bHLH142 and EAT1 can form a heterodimer with TDR1 with a favorable match and form a similar interface. We also predicted a favorable DNA binding pocket on the bHLH142/TDR1 heterodimer to bind to the specific E-box sequences (CAATTG) on the promoter of *EAT1* to trigger its transcription (Figure 10). Presumably, once the dimer binds to the E-box, the nucleotide base pairs on both ends of the DNA molecule begin to dissociate and loosen the DNA helix structure for transcriptional activation. These modeling results are consistent with our Y2H data in this study that suggest that bHLH142 interacts with the C-terminal of TDR1 (Figure 8) and our transient promoter assay that demonstrated that simultaneous expression of bHLH142 and TDR1 is required for the expression of *EAT1* (Figure 7). The predicted dimerization between EAT1 and TDR1 (Figure 9) is also consistent with the data of Niu et al. (2013) and Ji et al. (2013), who showed from Y2H analysis that TDR1 can interact with EAT1. Our modeling suggests that EAT1 competes well with bHLH142, binding to TDR1 in a similar manner with a comparable binding

free energy. Therefore, we propose that the interaction between bHLH142 and TDR1 promotes the expression of *EAT1*, which in turn interacts with TDR1 and serves as a feedback inhibitor of *EAT1* transcription. In agreement with this proposal, simultaneous expression of both bHLH142 and TDR1 largely enhanced *EAT1* expression, while additional expression of EAT1 along with bHLH142 and TDR1 competitively reduced the expression of *EAT1* (Figure 7). Our genetic study clearly showed that the *bHLH142* knockout mutant has significantly lower *EAT1* mRNA as shown by qRT-PCR analysis (Figure 6F). Taken together, our modeling results are consistent with our experimental data in supporting the pivotal role of bHLH142 in *EAT1* expression and male sterility in rice. Whether EAT1/TDR1 heterodimer has other biological functions in gene regulation requires further investigation.

The Regulatory Cascade of Tapetal PCD in Rice

Based on this study and previous studies, an updated regulatory network for rice pollen development is presented in Figure 11. Previous work with various rice MS mutants suggests that UDT1 and GAMYB may positively regulate the transcription of *TDR1* (Liu et al., 2010), and TDR1 controls the transcription of *C6* and *CP1* (Li et al., 2006a). Recently, Niu et al. (2013) presented evidence that TDR1 interacts with EAT1 and that EAT1 directly regulates the expression of two aspartic proteases for initiation of tapetal PCD. In this study, we demonstrate that bHLH142 acts downstream of UDT1, but upstream of TDR1 and EAT1, and then bHLH142 interacts with TDR1 to activate *EAT1* transcription by binding to its promoter. In addition, we also provide evidence that EAT1 may directly regulate the expression of *CP1*. Therefore, we conclude that bHLH142 is essential for tapetal PCD and pollen development in rice.

Application of Genetic Male Sterility in Hybrid Crop Production

Crops produced from F1 hybrid seeds offer significant benefits in terms of yield improvement, agronomic performance, and consistency of end-use quality. This is due to the hybrid vigor

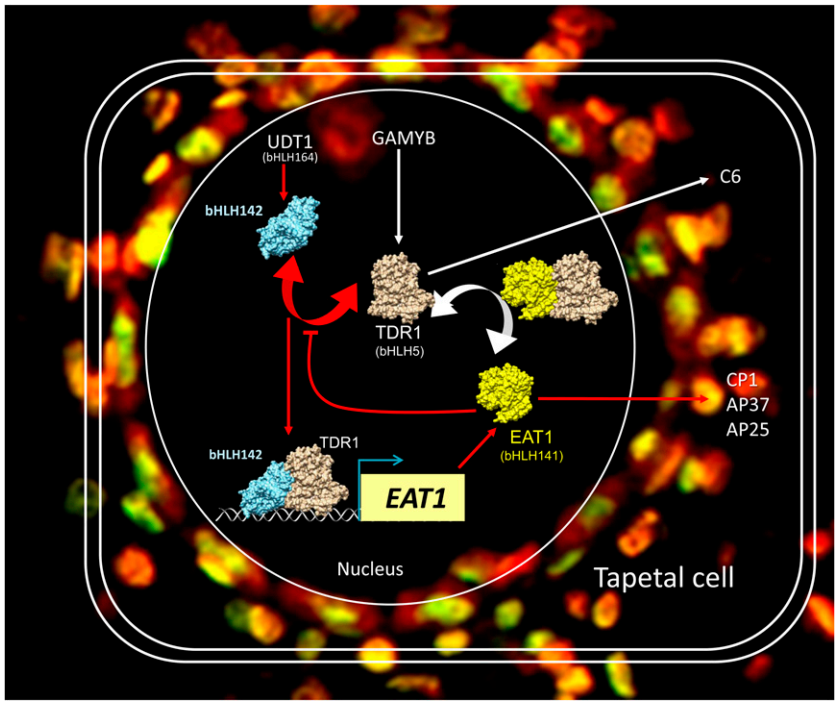

Figure 11. The Regulatory Cascade of Tapetal PCD in Rice.

The model depicts the molecular function of bHLH142 in rice anther development, relative to other known key regulators. bHLH142 acts downstream of UDT1 but upstream of TDR1 and by interacting with TDR1 to form a heterodimer (Figure 9). Both bHLH142 and TDR1 coordinately regulate the expression of *EAT1* by binding its promoter (Figure 8). In turn, EAT1 interacts with TDR1 (Ji et al., 2013; Niu et al., 2013) and forms a heterodimer in a similar manner (Figure 9). Thus, EAT1 competes with bHLH142 for the similar protein binding sites on TDR1 with a comparable binding free energy (Figure 9); therefore, feedback inhibits bHLH142/TDR1 interaction and *EAT1* expression (Figure 7). Previous studies suggest that TDR1 acts downstream of UDT1 and GAMYB and that UDT1 and GAMYB work in parallel to regulate early stage anther development (Liu et al., 2010). TDR1 directly regulates the expression of *C6* and *CP1* that encode cysteine protease and protease inhibitor, respectively (Li et al., 2006a), while EAT1 regulates the expression of two aspartic proteases (AP37 and AP25) and promotes tapetal PCD during anther development (Niu et al., 2013). This study also provides evidence that EAT1 may directly regulate the expression of *CP1*. Evidence from previous studies is indicated by white arrows, while data demonstrated in this study are indicated by red arrows. The background is TUNEL signal in anther of TNG67 at the young microspore stage. The red signal is propidium iodide staining, and yellow fluorescence is the merged signal from TUNEL (green) and propidium iodide.

generated by combining carefully selected parent lines. Hybrid crops are responsible for the dramatic increase in global crop yields in recent decades, and male-sterile traits have played a significant role in this advancement. CMS, a maternally inherited trait, has been widely exploited for hybrid crop breeding (e.g., maize and rice) due to the convenience of controlling sterility expression by manipulating the gene-cytoplasm combinations in any selected genotype. Most importantly, it eliminates the need for emasculation in cross-pollinated species, thus encouraging cross breeding, producing pure hybrid seeds under natural conditions. However, commercial seed production must be simple and inexpensive, and the requirement for a maintainer line to produce the seed stocks of the CMS line increases the production cost for this three-line hybrid system.

GMS, controlled by nuclear genes, offers an alternative hybrid seed production system. For the two-line hybrid system, it is beneficial to use photoperiod- or temperature-inducible male sterility (PGMS or TGMS) mutants to maintain seed stocks for hybrid seed production. In China, PA64S is currently the most widely used maternal line in two-line hybrid rice breeding. It is crossed with paternal line 93-11 to generate superhybrid rice, LYP9 (Luo et al., 1992). PA64S, derived from a spontaneous PGMS *japonica* mutant NK58S (long day, >13.5 h; Shi, 1985), is also a TGMS *indica* rice, whose male sterility is promoted by temperatures greater than 23.5°C, but recovers its fertility at temperatures between 21 and 23°C. Recent mapping analyses demonstrate that the PGMS/TGMS in these lines is regulated by a novel small RNA (Zhou et al., 2012). In another rice genic male-sterile mutant discovered recently, Carbon Starved Anther (CSA), a mutation of the *R2R3 MYB* transcription regulator results in a defect in pollen development (Zhang et al., 2010b). Further study of this mutant showed that *csa* is photoperiod-sensitive, exhibiting male sterility under short-day conditions but male fertility under long-day conditions (Zhang et al., 2013). The molecular basis of this sensitivity to daylength remains undetermined.

Transgenic male sterility has been generated using a number of transgenes, but its application in commercial production of hybrid seeds is limited due to the lack of an efficient and economical means to maintain the male sterile lines or the lack of suitable restorers (Li et al., 2007). Recently, a reversible male-sterile system has been demonstrated in transgenic *Arabidopsis* plants by manipulating a R2R3 MYB domain protein (MYB103) (Li et al., 2007). Blocking the function of MYB103 using an insertion mutant or an *MYB103EAR* chimeric repressor construct under the control of the *MYB103* promoter resulted in complete male sterility without seed setting (Li et al., 2007). A restorer containing the *MYB103* gene driven by a stronger anther-specific promoter was introduced into pollen donor plants and crossed into the male-sterile transgenic plants for the repressor restoring the male fertility of F1 plants. The chimeric repressor and the restorer constitute a reversible male-sterile system for hybrid seed production. The successful application of this system for large-scale hybrid seed production depends on whether the female parent lines can be multiplied efficiently and economically. Alternatively, a promoter inducible by chemicals or other factors (e.g., photoperiod or temperature) can be directly used to regulate the expression of a GMS gene (e.g., *bHLH142*) and control pollen development in transgenic plants, eliminating the costly need to maintain male-sterile lines.

METHODS

Plant Materials and Growth Conditions

Seeds of the *ms142* mutant were obtained from the TRIM library (http://trim.sinica.edu.tw/). Seedlings of *ms142* mutant and its wild type (TNG67) were raised in half-strength Kimura solution for 3 weeks and then transplanted into soil in the Academia Sinica-Biotechnology Center in Southern Taiwan screen house for genetically modified organisms, located in Tainan, Taiwan.

Anther Anatomy

Spikelets and anthers of the wild type and *ms142* mutant were sampled at various stages of development and fixed overnight in phosphate buffer (pH 7.0) that contained 4% paraformaldehyde and 2.5% glutaraldehyde. They were then rinsed with the same buffer and postfixed for 30 min in phosphate buffer, pH 7.0, containing 1% osmium tetroxide. After dehydration, the specimens were embedded in Spurr's Resin (EMS). The processor, KOS Rapid Microwave Labstation, was chosen for post-fixation, dehydration, resin infiltration, and embedding. For TEM, ultrathin sections (90 to 100 nm thick) collected on coated copper grids were stained with 6% uranyl acetated and 0.4% lead citrate and examined using transmission electron microscope.

Meiotic Analysis

For meiotic studies, young spikelets of the wild type and *ms142* at 2- to 4-mm length stages were fixed with ethanol:acetic acid (3:1, v/v) overnight, then transferred to 70% ethyl alcohol and stored under refrigeration. Meiotic chromosome spreads were prepared following the protocol described previously (Chang et al., 2009b) with some modifications. In brief, anthers were dissected gently with forceps and needles and transferred to a glass slide together with a drop of 1% acetocarmine and squashed gently with a needle to release MMCs; and the anther wall debris was carefully removed before a cover slip was added. Finally, the preparation was gently squashed by vertical press and analyzed under microscopy (Zeiss Axio Scope A1). Photographs were taken using Axio-Cam HRc camera (Zeiss).

TUNEL Assay

PCD is characterized by cellular condensation, mitochondria and cytoskeleton degeneration, nuclear condensation, and internucleosomal cleavage of chromosomal DNA (Phan et al., 2011). To investigate the nature of the tapetal breakdown in *ms142*, TUNEL assay was performed using the DeadEnd Fluorometric TUNEL system (Promega). This assay detects in situ DNA cleavage, a hallmark feature of apoptosis-like PCD, by enzymatically incorporating fluorescein-12-dUTP into the 3′-OH ends of fragmented DNA. Stage of anther development was based primarily on spikelet size and developmental stages.

Total RNA Isolation and PCR

Total RNA was isolated from rice (*Oryza sativa*) tissues using MaestroZol RNA PLUS (Invitrogen) as described by the supplier. Various rice organs at different developmental stages were harvested for RNA isolation: root, shoot, flag leaf, internode, and panicles of 0.5, 1, 5, 9, 20 cm length, spikelets at 1 d before anthesis, lemma, palea, anthers, ovary, and seeds at 5 d after pollination (S1), 15 d after pollination (S3), 25 d after pollination

(S5), and calli. The stages of anthers were classified into the following categories according to spikelet length: MMC with spikelet length of ~2 mm, meiosis (4 mm), young microspore (YM, 6 mm), vacuolated pollen (VP, 8 mm), mitosis pollen (MP, 8 mm with light-green lemma), and mature pollen at 1 d before anthesis. Total RNA was treated with DNase (Promega), and 1 μg RNA was used to synthesize the oligo(dT) primed first-strand cDNA using the M-MLV reverse transcriptase cDNA synthesis kit (Promega). One microliter of the reverse transcription products was used as a template in the PCR reactions. *Ubiquitin-like 5* and *18srRNA* were used as normalizer control. Each sample had three biological repeats.

qRT-PCR Analysis

Fifteen microliters of RT-PCR reaction contained 4 μL of 1/4 diluted cDNA, 3 μM of primers, and 7.5 μL of 2X KAPA SYBR FAST master mix (KAPA Biosystems, USA). Real-Time PCR was performed using a CFX96 Real-Time PCR detection system (Bio-Rad, USA). Quantification analysis was performed using CFX Manager Software (Bio-Rad, USA). Primers used for qPCR are listed in Supplemental Table 4.

In Situ Hybridization

Spikelets of TNG67 and *ms142* at various developmental stages were collected and fixed, dehydrated, embedded, sliced, and performed hybridization as previously described (Lin et al., 2014). For preparation of digoxigenin-labeled RNA probes, we cloned the gene-specific region of *bHLH142* using primers listed in Supplemental Table 4.

Subcellular Localization of bHLH142

For subcellular localization of bHLH142, the coding sequences of the gene were subcloned into *p*2FGW7 (Invitrogen) to generate bHLH142-GFP fusion genes driven by the cauliflower mosaic virus 35S (CaMV35S) promoter. Rice protoplasts were isolated and transformed using the polyethylene glycol method following procedures described previously (Bart et al., 2006). After incubation at room temperature for 16 h in light, protoplasts were observed with a Zeiss LSM 780 confocal laser scanning microscope.

Phylogenetic Analysis of the bHLH142 Subfamily

The bHLH142 protein sequence was used to search for the closest homologs from the plant species using BLASTP programs. Multiple sequence alignment of full-length protein sequences was performed using ClustalW online (http://www.ch.embnet.org/software/ClustalW.html), and the alignment was used to perform neighbor-joining analysis using Mega 5.05 (Tamura et al., 2011). The numbers at the nodes represent percentage bootstrap values based on 1000 replications. The length of the branches is proportional to the expected numbers of amino acid substitutions per site. Gene accession numbers of the sequences used to generate the phylogenetic tree and the alignment can be found as Supplemental Data Set 1.

Rice Protoplast Transient Expression and Reporter Gene Activity Assay

Transient promoter assay was performed as previously described (Li et al., 2011) with some modifications. In brief, protoplasts were isolated from leaf tissue of 10-d-old rice seedlings. The reporter plasmid contained the CaMV35S minimal promoter and the *EAT1* promoter (2031 bp) fused to the firefly luciferase gene (*Luc*). In the effector plasmids, bHLH142, TDR1, and EAT1 genes were under the control of the CaMV35S promoter. The pBI221 vector contained a CaMV35S promoter for driving the expression of GUS as an internal control.

Y2H Assay

The Matchmaker GAL4 two-hybrid system (Clontech) was used for Y2H assays. Since both full-length EAT1 and TDR1 proteins were reported to have self-activation (Ji et al., 2013), we made a truncated EAT1 (EAT1$^{\Delta}$, amino acids 1 to 254) and a truncated TDR1 (TDR$^{\Delta}$, amino acids 1 to 344) to reduce self-activation. The full-length cDNA of *bHLH142* was cloned into *p*GAD-T7 (Clontech), and full-length *bHLH142*, *EAT1*, *TDR, EAT1*$^{\Delta}$, and *TDR*$^{\Delta}$ were cloned into *p*GBK-T7 (Clontech), respectively. The pairs of constructs to be tested were cotransformed into AH109 yeast cells and selected on plates containing Leu (for *p*GADT7 plasmid) and Trp (for *p*GBKT7 plasmid) dropout medium for 3 to 4 d at 30°C. Transformants were tested for specific protein interactions by growing on SD/–Leu/–Trp/–His plates with 30 mM 3-amino-1,2,4 triazole and tested after X-α-Gal induction to confirm positive interaction. This system provides a transcriptional assay for detecting and confirming protein interactions in vivo in yeast.

BiFC Assay

BiFC assay allows visualization of protein–protein interactions in living cells and the direct detection of the protein complexes in subcellular compartments, providing insights into their functions. Full-length cDNAs of bHLH142, TDR1, and EAT1 were independently introduced into *p*JET1.2 (Thermo Scientific). The sequence for the N-terminal amino acid residues 1 to 174 of YFP was then in-frame fused to the sequence of the C-terminal region of the tested proteins, while the sequence of the C-terminal amino acid residues 175 to 239 of YFP was in-frame fused to the sequence of the N-terminal end of the proteins. Next, the tested genes were introduced into *p*SAT5-DEST_CYN1 and *p*SAT4(A)-DEST_NYN1. Ballistic bombardment-mediated transient transformation in rice protoplasts was performed following a previously published protocol (Hsu et al., 2011). Florescence images were photographed on a LSM 780 Plus ELYRA S.1 confocal microscope with a Plan-Apochromat 40×/1.4 oil objective lens (Zeiss).

Co-IP Assay

Recombinant proteins of bHLH142 and TDR1 fused with HA tag were expressed in bacteria harboring pET-53-DEST (HIS-tag), and cell extracts after lysis were centrifuged at 12,000 rpm for 15 min, suspended in binding buffer (20 mM Tris-HCl, pH 7.9, and 500 mM NaCl), and sonicated on ice for 30 s using an ultrasonic homogenizer (Misonix XL Sonicator Ultrasonic Cell Processor). The supernatants were purified using Ni^{2+} resin. For immunoprecipitation, extracts were precleared by 30 min incubation with 20 μL of PureProteome Protein G Magnetic Beads (Millipore) at 4°C with rotation. The antibodies (anti-bHLH142 or anti-HA) were then added to the precleared extracts. After incubation for 4 h at 4°C, 40 μL of PureProteome Protein G Magnetic Beads was added, and the extracts were further incubated for 10 min at room temperature with rotation. After extensive washing, bound proteins were analyzed by immunoblotting. Rabbit antiserum against rice bHLH142 was produced using a synthetic peptide (CSPTPRSGGGRKRSR) as antigen (GenScript).

Prediction of 3D Protein Structure and Interaction by Molecular Dynamics Simulation

3D protein structures were constructed by MD simulation using ab initio modeling methods. MD simulation was performed with the program NAMD (Nelson et al., 1996) using parameters adopted from the CHARMM force field (Brooks et al., 1983). The full-length protein sequences of EAT1 (NP_001053749.1), bHLH142 (NP_001042795.1), and TDR1

(NP_001045710.1) were obtained from the National Center for Biotechnology Information database. The models were minimized by removing unfavorable contacts, brought to 310K by velocity rescaling, and equilibrated for 1 ns. Before any MD trajectory was run, 40 ps of energy minimization was performed to relax the conformational and structural tensions. The minimum structure was the starting point for MD simulation. For this purpose, the protein molecule was embedded into a water simulation box and a cutoff distance of 12 Å was employed for the nonbonded and electrostatic interactions. The heating process was performed from 0 to 310K through Langevin damping with a coefficient of 10 ps^{-1}. A time step of 2 fs was employed for rescaling the temperature. After 20 ps of heating to 310K, equilibration trajectories of 2 μs were recorded, which provided the data for the structural and thermodynamic evaluations. The equations of motion were integrated with the Shake algorithm with a time step of 1 fs. The modeling quality of 3D models was evaluated by MQAP (Fischer, 2006) and the CASP7 experiment methods of QA (Cozzetto et al., 2007). Figures displaying atomistic pictures of molecules were generated using UCSF Chimera (Pettersen et al., 2004). The KD hydrophobicity of amino acid patches on protein surface was labeled as described previously (Kyte and Doolittle, 1982).

RNAi-Mediated Gene Silencing of *bHLH142*

To generate an RNAi construct for suppressing the expression of *bHLH142*, a 149-bp fragment from the 5′ UTR of *bHLH142* was amplified by PCR with specific primers (Supplemental Table 4) and cloned into *p*ENTR (Invitrogen) to yield an entry vector *p*PZP200 hph-Ubi-bHLH142 RNAi-NOS (12,483 bp). The RNAi construct was transformed into wild-type (TNG67) rice calli via an *Agrobacterium tumefaciens*–mediated transformation system (Chan et al., 1993). Transgenic plants were regenerated from transformed calli by selection on hygromycin-containing medium.

Accession Numbers

Sequence data from this article can be found in the GenBank/EMBL database under the following accession numbers: *bHLH142* (Os01g0293100), protein (NP_001042795.1); *CP1* (Os04g0670500); and *C6* (Os11g0582500). Additional loci are presented in Supplemental Table 4.

Supplemental Data

The following materials are available in the online version of this article.

Supplemental Figure 1. Evidence of T-DNA Insertion in *ms142* Mutant.

Supplemental Figure 2. Meiotic Analysis and Expression of Meiotic Regulatory Genes in the Wild-Type and *ms142*.

Supplemental Figure 3. Differential Interference Contrast Image of Anther Cross Section Used for TUNEL Assay.

Supplemental Figure 4. Scheme of *bHLH142* Gene, Multiple Alignment, and Subcellular Localization of bHLH142 Fused with GFP.

Supplemental Figure 5. Phylogenetic Analysis of bHLH142-Related Proteins.

Supplemental Figure 6. Real-Time PCR Analysis of Relative Gene Expression of *bHLH142* mRNA in the Anthers of *ms142*, *udt1*, *eat1*, and the Expression of *CP1* and *C6* in *eat1* Anther.

Supplemental Figure 7. Analysis of Protein Interaction between bHLH142, TDR1, and EAT1.

Supplemental Figure 8. RNAi Knockdown of *bHLH142* Inhibited Pollen Development.

Supplemental Table 1. Agronomic Traits and Grain Yields of *ms142* Mutant and Its BCF2 Population.

Supplemental Table 2. Genetic Determination of Male Fertility in *ms142* Mutant in Different Cropping Seasons.

Supplemental Table 3. Homologs of bHLH142 in Other Cereal Crops.

Supplemental Table 4. Primers Used in This Study.

Supplemental Data Set 1. Text File of Alignment Used to Generate Phylogenetic Tree in Supplemental Figure 5.

ACKNOWLEDGMENTS

We thank Su-May Yu, Yue-Ie Hsing, Chyr-Guan Chern, and Ming-Jen Fan for helping generate the TRIM database. We thank Yih-Jong Huang, Chai-Wei Kuo, and Ming-Sheng Lee for technical support. We also thank Choun-Sea Lin at the Plant Technology Core Facility of Academia Sinica for his assistance in transient expression and Shu-Chen Shen at the Confocal Microscope Core facility of Academia Sinica for her assistance in microscopy. We thank the DNA Sequencing Core Facility of Institute of Biomedical Sciences of Academia Sinica for providing DNA sequencing services. This work was supported by the Biotechnology Center in Southern Taiwan, Academia Sinica, and partly by the National Science Council of Taiwan (NSC 101-2313-B-001-003).

AUTHOR CONTRIBUTIONS

S.-S.K. identified mutants and designed the research. M.-J.L., Y.-C.H., Y.-J.L., Y.C.L., M.-H.C., H.-T.Y., H.-X.H., and H.-C.C. performed the experiments. S.-S.K., M.-J.L., Y.-C.H., and Y.-J.L. analyzed the data. M.-T.C. provided vectors and suggested molecular study. S.-S.K., M.S.-B.K., M.-J.L., Y.-C.H., and M.-H.C. wrote the article. M.S.-B.K. edited the article.

Received April 7, 2014; revised May 7, 2014; accepted May 13, 2014; published June 3, 2014.

REFERENCES

Aya, K., Suzuki, G., Suwabe, K., Hobo, T., Takahashi, H., Shiono, K., Yano, K., Tsutsumi, N., Nakazono, M., Nagamura, Y., Matsuoka, M., and Watanabe, M. (2011). Comprehensive network analysis of anther-expressed genes in rice by the combination of 33 laser microdissection and 143 spatiotemporal microarrays. PLoS ONE **6:** e26162.

Aya, K., Ueguchi-Tanaka, M., Kondo, M., Hamada, K., Yano, K., Nishimura, M., and Matsuoka, M. (2009). Gibberellin modulates anther development in rice via the transcriptional regulation of GAMYB. Plant Cell **21:** 1453–1472.

Bailey, P.C., Martin, C., Toledo-Ortiz, G., Quail, P.H., Huq, E., Heim, M.A., Jakoby, M., Werber, M., and Weisshaar, B. (2003). Update on the basic helix-loop-helix transcription factor gene family in *Arabidopsis thaliana*. Plant Cell **15:** 2497–2502.

Bart, R., Chern, M., Park, C.J., Bartley, L., and Ronald, P.C. (2006). A novel system for gene silencing using siRNAs in rice leaf and stem-derived protoplasts. Plant Methods **2:** 13.

Brooks, B.R., Bruccoleri, R.E., Olafson, B.D., States, D.J., Swaminathan, S., and Karplus, M. (1983). CHARMM: A program for macromolecular energy, minimization, and dynamics calculations. J. Comput. Chem. **4:** 187–217.

Carretero-Paulet, L., Galstyan, A., Roig-Villanova, I., Martínez-García, J.F., Bilbao-Castro, J.R., and Robertson, D.L. (2010). Genome-wide classification and evolutionary analysis of the bHLH

family of transcription factors in Arabidopsis, poplar, rice, moss, and algae. Plant Physiol. **153:** 1398–1412.

Chan, M.T., Chang, H.H., Ho, S.L., Tong, W.F., and Yu, S.M. (1993). Agrobacterium-mediated production of transgenic rice plants expressing a chimeric alpha-amylase promoter/beta-glucuronidase gene. Plant Mol. Biol. **22:** 491–506.

Chang, L., Ma, H., and Xue, H.W. (2009a). Functional conservation of the meiotic genes SDS and RCK in male meiosis in the monocot rice. Cell Res. **19:** 768–782.

Chang, Y., Gong, L., Yuan, W., Li, X., Chen, G., Li, X., Zhang, Q., and Wu, C. (2009b). Replication protein A (RPA1a) is required for meiotic and somatic DNA repair but is dispensable for DNA replication and homologous recombination in rice. Plant Physiol. **151:** 2162–2173.

Cozzetto, D., Kryshtafovych, A., Ceriani, M., and Tramontano, A. (2007). Assessment of predictions in the model quality assessment category. Proteins **69** (suppl. 8)**:** 175–183.

Fischer, D. (2006). Servers for protein structure prediction. Curr. Opin. Struct. Biol. **16:** 178–182.

Gao, Z.Y., et al. (2013). Dissecting yield-associated loci in super hybrid rice by resequencing recombinant inbred lines and improving parental genome sequences. Proc. Natl. Acad. Sci. USA **110:** 14492–14497.

Goldberg, R.B., Beals, T.P., and Sanders, P.M. (1993). Anther development: basic principles and practical applications. Plant Cell **5:** 1217–1229.

Higginson, T., Li, S.F., and Parish, R.W. (2003). AtMYB103 regulates tapetum and trichome development in Arabidopsis thaliana. Plant J. **35:** 177–192.

Hsing, Y.I., et al. (2007). A rice gene activation/knockout mutant resource for high throughput functional genomics. Plant Mol. Biol. **63:** 351–364.

Hsu, C.T., Liao, D.C., Wu, F.H., Liu, N.T., Shen, S.C., Chou, S.J., Tung, S.Y., Yang, C.H., Chan, M.T., and Lin, C.S. (2011). Integration of molecular biology tools for identifying promoters and genes abundantly expressed in flowers of Oncidium Gower Ramsey. BMC Plant Biol. **11:** 60.

Ito, T., and Shinozaki, K. (2002). The MALE STERILITY1 gene of Arabidopsis, encoding a nuclear protein with a PHD-finger motif, is expressed in tapetal cells and is required for pollen maturation. Plant Cell Physiol. **43:** 1285–1292.

Ito, T., Nagata, N., Yoshiba, Y., Ohme-Takagi, M., Ma, H., and Shinozaki, K. (2007). Arabidopsis MALE STERILITY1 encodes a PHD-type transcription factor and regulates pollen and tapetum development. Plant Cell **19:** 3549–3562.

Ji, C., Li, H., Chen, L., Xie, M., Wang, F., Chen, Y., and Liu, Y.G. (2013). A novel rice bHLH transcription factor, DTD, acts coordinately with TDR in controlling tapetum function and pollen development. Mol. Plant **6:** 1715–1718.

Jung, K.H., Han, M.J., Lee, Y.S., Kim, Y.W., Hwang, I., Kim, M.J., Kim, Y.K., Nahm, B.H., and An, G. (2005). Rice Undeveloped Tapetum1 is a major regulator of early tapetum development. Plant Cell **17:** 2705–2722.

Kawanabe, T., Ariizumi, T., Kawai-Yamada, M., Uchimiya, H., and Toriyama, K. (2006). Abolition of the tapetum suicide program ruins microsporogenesis. Plant Cell Physiol. **47:** 784–787.

Khush, G.S. (2000). Rice germplasm enhancement at IRRI Phillipp. J. Crop Sci. **25:** 45–51.

Kyte, J., and Doolittle, R.F. (1982). A simple method for displaying the hydropathic character of a protein. J. Mol. Biol. **157:** 105–132.

Lee, S., Jung, K.H., An, G., and Chung, Y.Y. (2004). Isolation and characterization of a rice cysteine protease gene, OsCP1, using T-DNA gene-trap system. Plant Mol. Biol. **54:** 755–765.

Li, C.W., Su, R.C., Cheng, C.P., Sanjaya, You, S.J., Hsieh, T.H., Chao, T.C., and Chan, M.T. (2011). Tomato RAV transcription factor is a pivotal modulator involved in the AP2/EREBP-mediated defense pathway. Plant Physiol. **156:** 213–227.

Li, H., Pinot, F., Sauveplane, V., Werck-Reichhart, D., Diehl, P., Schreiber, L., Franke, R., Zhang, P., Chen, L., Gao, Y., Liang, W., and Zhang, D. (2010). Cytochrome P450 family member CYP704B2 catalyzes the ω-hydroxylation of fatty acids and is required for anther cutin biosynthesis and pollen exine formation in rice. Plant Cell **22:** 173–190.

Li, N., et al. (2006a). The rice tapetum degeneration retardation gene is required for tapetum degradation and anther development. Plant Cell **18:** 2999–3014.

Li, S.F., Iacuone, S., and Parish, R.W. (2007). Suppression and restoration of male fertility using a transcription factor. Plant Biotechnol. J. **5:** 297–312.

Li, X., et al. (2006b). Genome-wide analysis of basic/helix-loop-helix transcription factor family in rice and Arabidopsis. Plant Physiol. **141:** 1167–1184.

Lin, H.Y., Chen, J.C., Wei, M.J., Lien, Y.C., Li, H.H., Ko, S.S., Liu, Z.H., and Fang, S.C. (2014). Genome-wide annotation, expression profiling, and protein interaction studies of the core cell-cycle genes in Phalaenopsis aphrodite. Plant Mol. Biol. **84:** 203–226.

Liu, Z., Bao, W., Liang, W., Yin, J., and Zhang, D. (2010). Identification of gamyb-4 and analysis of the regulatory role of GAMYB in rice anther development. J. Integr. Plant Biol. **52:** 670–678.

Luo, D., et al. (2013). A detrimental mitochondrial-nuclear interaction causes cytoplasmic male sterility in rice. Nat. Genet. **45:** 573–577.

Luo, X.H., Qiu, Z.Z., and Li, R.H. (1992). Pei'ai 64S, a dual-purpose sterile line whose sterility is induced by low critical temperature. Hybrid Rice **1:** 27–29.

Massari, M.E., and Murre, C. (2000). Helix-loop-helix proteins: regulators of transcription in eucaryotic organisms. Mol. Cell. Biol. **20:** 429–440.

Nelson, M., Humphrey, W., Gursoy, A., Dalke, A., Kale´, L., and Skeel, R.D. (1996). NAMD- A parallel, object-oriented molecular dynamics program. Int. J. Supercomput. Appl. High Perform. Comput. **10:** 251–256.

Niu, N., Liang, W., Yang, X., Jin, W., Wilson, Z.A., Hu, J., and Zhang, D. (2013). EAT1 promotes tapetal cell death by regulating aspartic proteases during male reproductive development in rice. Nat. Commun. **4:** 1445.

Nonomura, K., Morohoshi, A., Nakano, M., Eiguchi, M., Miyao, A., Hirochika, H., and Kurata, N. (2007). A germ cell specific gene of the ARGONAUTE family is essential for the progression of premeiotic mitosis and meiosis during sporogenesis in rice. Plant Cell **19:** 2583–2594.

Nonomura, K., Nakano, M., Fukuda, T., Eiguchi, M., Miyao, A., Hirochika, H., and Kurata, N. (2004). The novel gene HOMOLOGOUS PAIRING ABERRATION IN RICE MEIOSIS1 of rice encodes a putative coiled-coil protein required for homologous chromosome pairing in meiosis. Plant Cell **16:** 1008–1020.

Papini, A., Mosti, S., and Brighigna, L. (1999). Programmed-cell-death events during tapetum development of angiosperms. Protoplasma **207:** 213–221.

Pettersen, E.F., Goddard, T.D., Huang, C.C., Couch, G.S., Greenblatt, D.M., Meng, E.C., and Ferrin, T.E. (2004). UCSF Chimera—a visualization system for exploratory research and analysis. J. Comput. Chem. **25:** 1605–1612.

Phan, H.A., Iacuone, S., Li, S.F., and Parish, R.W. (2011). The MYB80 transcription factor is required for pollen development and the regulation of tapetal programmed cell death in *Arabidopsis thaliana*. Plant Cell **23:** 2209–2224.

Ptashne, M. (1988). How eukaryotic transcriptional activators work. Nature **335:** 683–689.

Rasheva, V.I., and Domingos, P.M. (2009). Cellular responses to endoplasmic reticulum stress and apoptosis. Apoptosis **14:** 996–1007.

Shi, M. (1985). The discovery and preliminary studies of the photoperiod-sensitive recessive male sterile rice (*Oryza sativa* L. subsp. japonica). Sci. Agric. Sin. **18:** 44–48.

Sorensen, A.M., Kröber, S., Unte, U.S., Huijser, P., Dekker, K., and Saedler, H. (2003). The Arabidopsis ABORTED MICROSPORES (AMS) gene encodes a MYC class transcription factor. Plant J. **33:** 413–423.

Stormo, G.D., and Fields, D.S. (1998). Specificity, free energy and information content in protein-DNA interactions. Trends Biochem. Sci. **23:** 109–113.

Tamura, K., Peterson, D., Peterson, N., Stecher, G., Nei, M., and Kumar, S. (2011). MEGA5: molecular evolutionary genetics analysis using maximum likelihood, evolutionary distance, and maximum parsimony methods. Mol. Biol. Evol. **28:** 2731–2739.

Toledo-Ortiz, G., Huq, E., and Quail, P.H. (2003). The Arabidopsis basic/helix-loop-helix transcription factor family. Plant Cell **15:** 1749–1770.

Wilson, Z.A., Morroll, S.M., Dawson, J., Swarup, R., and Tighe, P.J. (2001). The Arabidopsis MALE STERILITY1 (MS1) gene is a transcriptional regulator of male gametogenesis, with homology to the PHD-finger family of transcription factors. Plant J. **28:** 27–39.

Wu, H.M., and Cheun, A.Y. (2000). Programmed cell death in plant reproduction. Plant Mol. Biol. **44:** 267–281.

Yuan, W., Li, X., Chang, Y., Wen, R., Chen, G., Zhang, Q., and Wu, C. (2009). Mutation of the rice gene PAIR3 results in lack of bivalent formation in meiosis. Plant J. **59:** 303–315.

Zhang, D., Liang, W., Yin, C., Zong, J., Gu, F., and Zhang, D. (2010a). OsC6, encoding a lipid transfer protein, is required for postmeiotic anther development in rice. Plant Physiol. **154:** 149–162.

Zhang, H., Liang, W., Yang, X., Luo, X., Jiang, N., Ma, H., and Zhang, D. (2010b). Carbon starved anther encodes a MYB domain protein that regulates sugar partitioning required for rice pollen development. Plant Cell **22:** 672–689.

Zhang, H., Xu, C., He, Y., Zong, J., Yang, X., Si, H., Sun, Z., Hu, J., Liang, W., and Zhang, D. (2013). Mutation in CSA creates a new photoperiod-sensitive genic male sterile line applicable for hybrid rice seed production. Proc. Natl. Acad. Sci. USA **110:** 76–81.

Zhang, W., Sun, Y., Timofejeva, L., Chen, C., Grossniklaus, U., and Ma, H. (2006). Regulation of Arabidopsis tapetum development and function by DYSFUNCTIONAL TAPETUM1 (DYT1) encoding a putative bHLH transcription factor. Development **133:** 3085–3095.

Zhou, H., et al. (2012). Photoperiod- and thermo-sensitive genic male sterility in rice are caused by a point mutation in a novel noncoding RNA that produces a small RNA. Cell Res. **22:** 649–660.

Zhu, J., Chen, H., Li, H., Gao, J.F., Jiang, H., Wang, C., Guan, Y.F., and Yang, Z.N. (2008). Defective in Tapetal development and function 1 is essential for anther development and tapetal function for microspore maturation in Arabidopsis. Plant J. **55:** 266–277.